12-1995

Dynamic Pulse Buckling of Columns with Viscous Damping

Murli Kadandale

DYNAMIC PULSE BUCKLING OF COLUMNS WITH VISCOUS DAMPING

by

Murli Kadandale

A Thesis
Submitted to the
Faculty of The Graduate College
in partial fulfillment of the
requirements for the
Degree of Master of Science in Engineering
Department of Mechanical and Aeronautical Engineering

Western Michigan University
Kalamazoo, Michigan
December 1995

ACKNOWLEDGMENTS

When I started with this research, I wasn't aware of the kind of problems that I would run into. There is an obvious lack of published material in the field of "pulse buckling". On the way there were some very disturbing and frustrating times. If it weren't for the expertise of my mentor, Dr. Judah Ari-Gur, and his support and advice, I am not sure if I could have come this far. Working under Dr. Ari-Gur has really been very enriching, and I would like to thank him for everything that he has done for me.

I would also like to thank Dr. Dennis Vandenbrink and Dr. Jim Kamman for agreeing to be on the thesis committee. The courses that I took under them prepared me, to a large extent, to tackle some of the problems encountered.

Last but not the least I would like to thank Mr. Sridhar Erra and rest of the employees of the CAE Laboratory for extending special favors to me, ranging from the use of the faculty room to "checking out" multiple terminals.

Murli Kadandale

DYNAMIC PULSE BUCKLING OF GEOMETRICALLY IMPERFECT COLUMNS WITH VISCOUS DAMPING

Murli Kadandale, M.S.E

Western Michigan University, 1995

This is a study of dynamic pulse buckling of columns with viscous damping. The differential equations of motion were obtained using the Bernoulli-Navier hypothesis. The effects of axial and rotary inertia were included in the analysis. The Voigt-Kelvin model for a viscoelastic material is used. The Finite Difference Method was employed to solve the differential equations of motion. First columns without geometrical imperfections were studied, and a correlation between the damping modulus and the more familiar damping ratio was obtained. Then beams with initial geometrical imperfection were studied. A suitable dynamic buckling criterion was defined. It was observed that viscous damping plays a significant role in buckling analysis under extremely short pulses. Columns could withstand extremely high load intensities for impulsive loading. Buckling under impulsive loading was observed to be very sensitive to geometrical imperfection. Rotary inertia did not significantly effect the buckling results.

TABLE OF CONTENTS

Table of Contents-Continued

LIST OF FIGURES

List of Figures - Continued

List of Figures - Continued

CHAPTER I

INTRODUCTION

Forms of Dynamic Buckling

Dynamic stability of structures is a very broad subject that includes not only dynamic buckling from transient and vibratory loads, but also interaction of structures with other media, such as in aircraft flutter, and interaction with active control systems that have their own dynamic characteristics.

There are different types of dynamic buckling that can be distinguished based on the physical phenomena of the buckling processes. A distinction in dynamic buckling can be made between buckling from oscillatory loads and buckling from transient loads consisting of a single pulse characterized by its pulse, shape, and duration. The first type may be called "vibration buckling" and the second, " pulse buckling".

In vibration buckling, the amplitudes of vibration caused by an oscillating load become unacceptably large at critical combinations of load amplitude, load frequency, and structure damping. Consider a column supporting an oscillating axial load. Inevitable imperfections in the column give rise to bending moments that excite lateral motion. The column oscillates with large amplitude when the loading frequency is

twice the natural bending frequency of the column. Each time the column bows out to one side or the other, the axial loading force reaches its maximum and produces bending moments. The term vibration buckling describes the similarity to vibration resonance. The difference is that in vibration resonance the load is the same direction as the motion and excites the motion directly as the forcing function in the equation of motion. Simple resonance occurs when the lateral loading frequency coincides with the natural frequency of vibration. By contrast, in vibration buckling the bending moment induced by the axial force introduces the force as a parameter multiplying the displacement in the equation of motion. A mathematical description of vibration buckling, also known as "parametric instability", is therefore: dynamic instability induced by oscillating loading. An extensive treatment of this subject is presented in a book by Bolotin.

In pulse buckling, the structure deforms to an unacceptably large amplitude as the result of a transient. The deformation can be either permanent, as a result of plastic response or snap through to a large-deformation post buckled state, or the structure can return to its undeformed state. Motion grows exponentially in all modes with wavelengths longer than the Euler wavelengths for the given load intensity. The critical modes are those with greatest total growth during the time of the load application (Lindberg and Florence, 1987). The critical condition for buckling is an unacceptably large deformation or stress. The column can survive a large axial load before reaching this condition if the load duration is short enough. Here load appears

as a parameter multiplying the displacement in the equations of motion. Mathematically this problem can be defined as: dynamic response of structural systems induced by time-varying loading. It is sought to study the pulse buckling of beams in this study.

Literature Survey

A considerable amount of work has been done in the field of dynamic pulse buckling of columns. One of the earliest studies on this subject was that of Koning and Taub (1933). They treated a column loaded by a constant axial compression for a specified period of time and showed that when the axial load is greater than the static buckling load the deflection increases exponentially with time. Meier (1945) showed that a column subjected to a rapidly applied axial stress may withstand compressive loads much greater than the static buckling load. These studies assume that the initial geometrical imperfection and the resulting deflection have the shape of a half sine wave. Also the effects of axial inertia were ignored. Axial inertia may be neglected in case of low rates of loading. This problem was studied by Hoff (1953) and Erickson et al. (1956), and was extended by Sevin (1960) to include axial inertia.

For loadings of short duration wave propagation phenomena become important. A customary manner of impulsive loading is by a collision with a striking mass. The analysis for the propagating stress field developing after impact is presented in textbooks, e.g. Goldsmith (1960). Hayashi and Sano (1972) investigated the

response of a column with initial geometrical imperfection impacted axially with a striking mass. They included axial inertia terms in their analysis, compared several beam theories and presented some test results. However, they did not define any dynamic buckling criterion.

Various experimental studies were conducted by Ari-Gur et al (1982) on clamped steel, aluminum alloy and glass epoxy columns. These experiments revealed distinct regions in the plots of maximum flexural response versus the peak magnitude of impulsive compression. In the first region the slope of the curve was quite moderate, while in the second a small increase in dynamic compression resulted in a much larger increase in the bending response. Buckling was defined to occur at the transition between these two distinct regions. A "Dynamic Load (Amplification) Factor (DLF)" was introduced. It was seen that material properties play only a secondary role in the determination of DLF. The numerical results from a finite difference program revealed close correlation with experimental results. A "generalized Southwell equation" was introduced to determine the upper bound of the response. In a theoretical study by Ari-Gur and Elishakoff (1993) it was shown that unless the transverse shear rigidity is extremely low (soft), its effects may be neglected.

A study of dynamic elastic buckling of simply supported bars under step loading was presented by Lindberg and Florence in their monograph (1987). They assumed linear strain and neglected axial and rotary inertia effects. A closed form solution assuming a product solution (by separating variables in space and time) was

presented. It was shown that motion is unstable for all load intensities greater than the Euler critical load. Further, for a pulse intensity greater than the static buckling load, it was shown that the solution tends to be hyperbolic as the pulse duration increases. A "preferred" wavelength of dynamic buckling that is directly proportional to the square root of the bending stiffness and inversely proportional to the square root of the pulse intensity, was obtained. Critical combinations of load intensity and impulse were presented.

Motivation

As polymers are replacing more and more traditional engineering materials there is a greater need to study their behavior under different loading environments. One of the main differences between metals and polymers is in their creep, stress relaxation and strain rate sensitivity characteristics. While in the case of metals these may be safely neglected for most engineering analysis, their effect may be particularly important in polymers.

A significant amount of work has been done in the field of quasi-static buckling of viscoelastic columns. Vinogradov (1987) used constitutive equations of linear viscoelastic theory of heredity type to investigate creep buckling of a column with initial imperfection.

Cederbaum and Mond (1992) studied the stability of viscoelastic columns under a periodic force, using the Boltzman superposition principle to obtain the constitutive equation, and time scaling to obtain an approximate solution.

However, to the best of our knowledge, there is no study of viscoelastic beams under dynamic pulses. In a pulse buckling problem creep and stress relaxation can be assumed to be insignificant due to extremely short duration of load application.It was therefore decided that a simple Voigt-Kelvin model be used to analyze this problem as it lays emphasis on the strain rate.

CHAPTER II

FORMULATION

Governing Equations

Consider a column of length L, thickness h, unit width and initial geometrical imperfection $w_0(x)$ that is subjected to an axial compression pulse $N_0(t)$, as in Figure 1. In response to the pulse load, the column deforms and transient axial displacements $u(x,t)$ and lateral deflections $w(x,t)-w_0(x)$ are generated. Assume the sign convention as in Figure 2. Using the Bernoulli-Navier hypothesis, that straight lines normal to the reference curve, remain straight and normal during deformation, the following equations of motion were derived:

$$N_{x,x} = \rho h \ddot{u} \tag{1}$$

and

$$(-M_{x,x} + N_x w_{,x} + \frac{1}{12}\rho h^3 \ddot{w}_{,x})_{,x} = \rho h \ddot{w} \tag{2}$$

where, ρ is the mass density, the force N_x and moment M_x per unit width are:

$$(N_x, M_x) = \int_{-h/2}^{h/2} \sigma(1,-z)dz \tag{3}$$

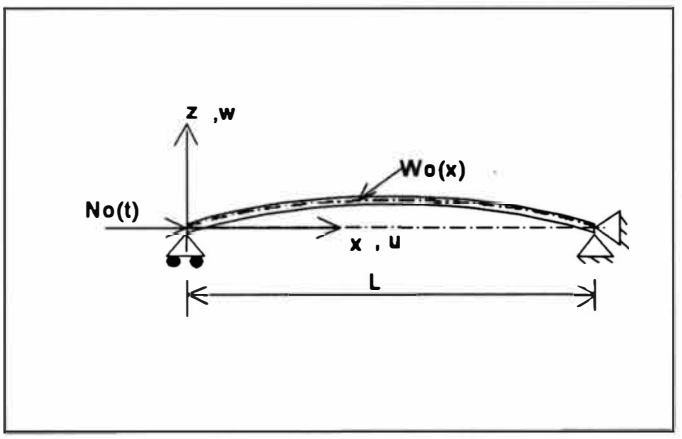

Figure 1. Geometrically Imperfect Beam Under an Axial Pulse.

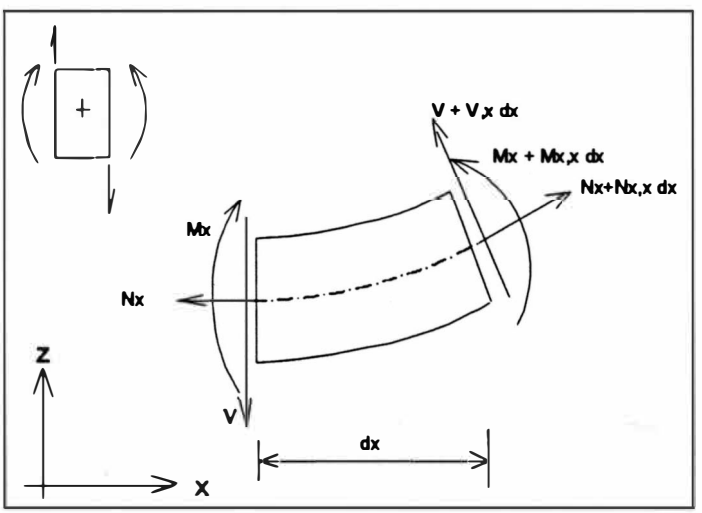

Figure 2. Loaded Element.

and $\sigma = \sigma(x,z,t)$ is the axial stress in the column. Note that $w_{,x}$ represents derivative of w with respect to "x", and the dots represent time derivatives.

Assuming a material with linear viscous damping (Voigt-Kelvin model), the constitutive equation is given by:

$$\sigma = E\varepsilon + \mu\dot{\varepsilon} \tag{4}$$

where E is the elastic modulus and μ is the dissipation modulus. The strain is:

$$\varepsilon = u_{,x} + \frac{1}{2}\{(w_{,x})^2 - (w_{0,x})^2\} \tag{5}$$

In Equation (5),

$$u_{,x} = u_{0,x} - (w - w_0)_{,xx} z \tag{6}$$

where u_0 is the axial displacement of the neutral line of the column. Using Equation (6), Equation (5) is written as:

$$\varepsilon = \varepsilon_x + \kappa_x z \tag{7}$$

where,

$$\varepsilon_x = u_{0,x} + \frac{1}{2}[(w_{,x})^2 - (w_{0,x})^2] \tag{8}$$

and

$$\kappa_x = -(w - w_0)_{,xx} \tag{9}$$

ε_x is the strain of the midplane of the column, κ_x is the curvature. Taking the derivative of Equation (7) with respect to time:

$$\dot{\varepsilon} = \dot{\varepsilon}_x + \dot{\kappa}_x z \tag{10}$$

Substituting Equations (7) and (10) in Equation (4), and then substituting the result in Equation (3), we get:

$$N_x = Eh\varepsilon_x + \mu h\dot{\varepsilon}_x \tag{11}$$

and

$$M_x = \frac{-h^3}{12}\{E\kappa_x + \mu\dot{\kappa}_x\} \tag{12}$$

Initial Conditions

Assuming that the beam is initially at rest, the conditions at time t = 0 are:

$$\varepsilon_x = \kappa_x = \dot{\varepsilon}_x = \dot{\kappa}_x = 0 \tag{13}$$

$$u = 0 \tag{14}$$

$$w = w_0 \tag{15}$$

Boundary Conditions

For the end x = L axially restrained:

$$u = 0 \quad \text{at } x = L \tag{16}$$

The axial displacement of the loaded end (x = 0) is dictated by the pulse force, hence:

$$N_x = -N_0(t) \quad \text{at } x = 0 \tag{17}$$

For simply supported ends:

$$w = 0, M_x = 0 \quad \text{at } x = 0, L \tag{18}$$

For clamped ends:

$$w = w_{,x} = 0 \qquad \text{at } x = 0, L \tag{19}$$

Finite Difference Approximation

Finite difference approximation was used to solve the differential equations of motion. The differential equations were approximated over finite time interval δt and axial element δx.

Central difference approximation was used for time derivatives in Equations (1) and (2). Using these approximations, explicit equations for u and w were obtained. The differential equations were then integrated by time stepping. Based on the approximation for ε_x and κ_x for the last two time steps, backward difference was used to estimate $\dot{\varepsilon}_x$ and $\dot{\kappa}_x$.

Central difference scheme was employed for spatial derivatives except for the end points. At x = 0 forward difference schemes and at x = L backward difference schemes were used for spatial derivatives.

A listing of the finite difference approximations is given below. These equations are based on the assumption of uniform segment size. In the equations, i and j represent the space and time coordinates respectively.

1. Estimation of ε_x and κ_x needs the following difference equations:

For the first node, i = 1 (forward difference scheme):

$$u_{,x}(1,j) = \frac{u(2,j) - u(1,j)}{\delta x} \tag{20.1}$$

$$w_{,x}(1,j) = \frac{w(2,j) - w(1,j)}{\delta x} \tag{20.2}$$

$$w_{,xx}(1,j) = \frac{w(3,j) - 2w(2,j) + w(1,j)}{2\delta x^2} \tag{20.3}$$

For the second to second to last (i = 2 to i = n-1):

$$u_{,x}(i,j) = \frac{u(i+1,j) - u(i-1,j)}{2\delta x} \tag{21.1}$$

$$w_{,x}(i,j) = \frac{w(i+1,j) - w(i-1,j)}{2\delta x} \tag{21.2}$$

$$w_{,xx}(i,j) = \frac{w(i+1,j) - 2w(i,j) + w(i-1,j)}{\delta x^2} \tag{21.3}$$

For the last node, i = n, (backward difference scheme):

$$u_{,x}(n,j) = \frac{u(n,j) - u(n-1,j)}{\delta x} \tag{22.1}$$

$$w_{,x}(n,j) = \frac{w(n,j) - w(n-1,j)}{\delta x} \tag{22.2}$$

$$w_{,xx}(n,j) = \frac{w(n-2,j) - 2w(n-1,j) + w(n-2,j)}{2\delta x^2} \tag{22.3}$$

2. Backward difference scheme was used for estimating the time derivatives $\dot{\varepsilon}_x$ and $\dot{\kappa}_x$:

$$\dot{\varepsilon}_x(i,j) = \frac{\varepsilon_x(i,j) - \varepsilon_x(i,j-1)}{\delta t} \tag{23.1}$$

$$\dot{\kappa}_x(i,j) = \frac{\kappa_x(i,j) - \kappa_x(i,j-1)}{\delta t} \tag{23.2}$$

3. The equations for ε_x ,κ_x, $\dot{\varepsilon}_x$ and $\dot{\kappa}_x$ are then used to estimate N_x and M_x. For estimation of u and w, we also need to find $N_{x,x}$ and $M_{x,xx}$, using the following:

For the first node (forward difference scheme):

$$N_{x,x}(1,j) = \frac{N_x(2,j) - N_x(1,j)}{\delta x} \tag{24.1}$$

$$M_{x,xx}(1,j) = \frac{M_x(3,j) - 2M_x(2,j) + M_x(1,j)}{2\delta x^2} \tag{24.2}$$

For nodes 2 to (n-1) using the central difference scheme:

$$N_{x,x}(i,j) = \frac{N_x(i+1,j) - N_x(i-1,j)}{2\delta x} \tag{25.1}$$

$$M_{x,xx}(i,j) = \frac{M_x(i+1,j) - 2M_x(i,j) + M_x(i-1,j)}{\delta x^2} \tag{25.2}$$

For the last node (backward difference scheme):

$$N_{x,x}(n,j) = \frac{N_x(n,j) - N_x(n-1,j)}{\delta x} \tag{26.1}$$

$$M_{x,xx}(n,j) = \frac{M_x(n,j) - 2M_x(n-1,j) + M_x(n-2,j)}{2\delta x^2} \tag{26.2}$$

4. The differential Equations (1) and (2) are written in the difference equation form (central difference scheme) to extrapolate u and w for the next time interval, j+1, as follows:

$$\frac{u(i,j+1) - 2u(i,j) + u(i,j-1)}{\delta t^2} = \frac{1}{\rho h} N_{x,x}(i,j) \tag{27}$$

$$\frac{w(i,j+1) - 2w(i,j) + w(i,j-1)}{\delta t^2} - \frac{h^2}{12}\left\{\frac{w_{,xx}(i,j+1) - 2w_{,xx}(i,j) + w_{,xx}(i,j-1)}{\delta t^2}\right\} = RHS \tag{28}$$

where,

$$RHS = \frac{1}{\rho h}\{-M_{x,xx}(i,j) + N_{x,x}w_{,x} + N_x w_{,xx}\} \tag{28.1}$$

To start the numerical solution the results for the first two steps are needed. The initial conditions, of the beam at rest, dictate the values of the variables 'u' and

'w' at t = 0. As will be explained later, the time step is sufficiently small so that due to wave propagation only the first node can move while $t \leq \delta t$. Hence, during the first time step ($t \leq \delta t$) only the first node experiences longitudinal motion (u), which is dictated by the load at that point. The axial strain ("fudged") during the first step is:

$$\varepsilon_x = \frac{N_x}{Eh + \frac{\mu h}{\delta t}} \tag{29}$$

Based on this, the displacement of the first node during the first time step is:

$$u = -\varepsilon_x c \delta t / 2 \; ; \; c = \sqrt{E / \rho} \tag{30}$$

where, c is the longitudinal wave propagation speed. The complete sets of values of 'u' and 'w' at t = 0 and t = δt are used to calculate $\varepsilon_x, \kappa_x, \dot{\varepsilon}_x$ and $\dot{\kappa}_x$ at t = δt. These are then used to calculate the values of nodal forces and moments, N_x and M_x respectively. These values are then used to find $N_{x,x}$ and $M_{x,xx}$. These, in turn, are substituted into the finite difference equations (27) and (28), to extrapolate the 'u' and 'w' values during the second time step (t = 2δt). Now the values from the second and the third time steps are used to extrapolate 'u' and 'w' for the fourth instant. This process is repeated to extrapolate 'u' and 'w' successively.

Computer Program Implementation

A code was written in BASIC to solve this problem. Figure 3 shows a logical flow chart. All float variables were defined as double precision values. The inputs are the material properties, the beam properties, the boundary conditions, the number of

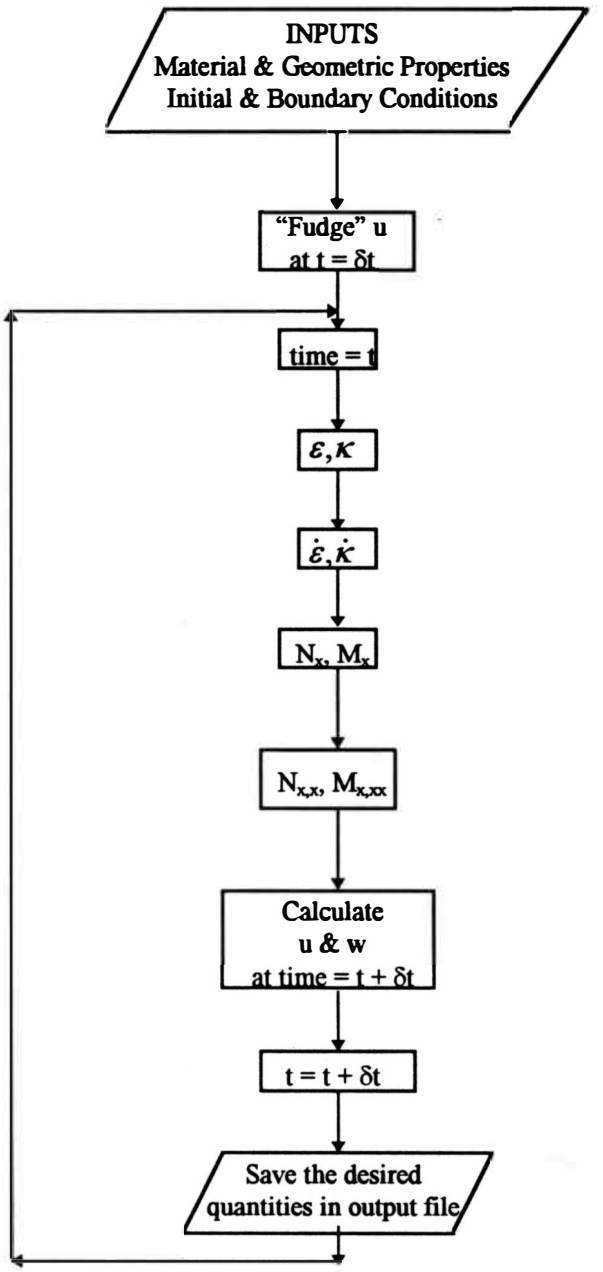

Figure 3. Flow Chart of the Computer Program.

segments (n) and the load specification.

As is evident;

'u' and 'w' must be defined as (n X 3) arrays

ε_x and κ_x must be defined as (n X 2) arrays

$\dot{\varepsilon}_x$, $\dot{\kappa}_x$, N_x and M_x must be defined as arrays of size 'n'.

The program also provides an option of including or excluding rotary inertia from the analysis by means of a flag which can be set at 1 or 0. If rotary inertia is included in the analysis then the program goes through a routine of Gaussian elimination and back substitution to extrapolate 'w'.A listing of the program is given in Appendix A. A program that accepts a data file with the nodal deflections (w) and displacements (u) at specified time intervals to animate the behavior of the column under impact is given in Appendix B.

The time interval chosen to assure numerical stability always satisfies the following (Smith, 1969):

$$\frac{\delta t}{\delta x}\sqrt{\frac{E}{\rho}} \leq 1 \tag{31}$$

This implies that the time step should be less than the time required for wave to propagate through a distance δx, for the solution to converge. In addition, it was observed here that the following empirical relationship was also required to guarantee convergence for all the results of this study:

$$\frac{\delta t}{\delta x}\sqrt{\frac{E}{\rho}} \le \frac{\sqrt{L/h}}{\left(10+\frac{\overline{\mu}}{25}\right)} \tag{32}$$

where $\overline{\mu}$ is the normalized viscous damping defined in the next section. This inequality becomes dominant when the ratio L/h decreases and $\overline{\mu}$ increases, so that:

$$\frac{\sqrt{L/h}}{\left(10+\frac{\overline{\mu}}{25}\right)} < 1 \tag{33}$$

Nondimensionalization

For the results to convey a more general meaning the following non-dimensional variables were used.

Load Ratio, that relates the pulse intensity and Euler critical load, is:

$$\overline{N} = N_0 / N_{cr} \tag{34}$$

where N_0 is the load intensity. N_{cr} is the Euler critical load given by:

$$N_{cr} = EA\varepsilon_{cr} \tag{35}$$

where A is the crossection area and ε_{cr} is the critical strain given by:

$$\varepsilon_{cr} = (\pi / \lambda_{eff})^2 \tag{36}$$

λ_{eff} is the effective slenderness ratio:

$$\lambda_{eff} = \frac{L\sqrt{A}}{\alpha\sqrt{I}} \tag{37}$$

where, I is the area moment of inertia. $\alpha = 1$ for simply supported ends and $\alpha = 2$ for clamped ends.

Duration Ratio relates the pulse duration and the fundamental flexural time period and is defined as:

$$\overline{T} = \omega T / \pi \tag{38}$$

where T is the pulse duration. The flexural fundamental frequency (Thomson, 1988) is:

$$\omega = K\sqrt{\frac{EI}{\rho A}} \tag{39}$$

where, K = 9.87 for simply supported ends and 22.4 for clamped ends.

Axial Duration Ratio relates the pulse duration to the fundamental longitudinal time period and is defined as:

$$T^{*} = \omega_{l} T / \pi \tag{40}$$

where, ω_l is the fundamental longitudinal frequency given by:

$$\omega_{l} = \frac{\pi}{L}\sqrt{\frac{E}{\rho}} \tag{41}$$

Non-dimensional Damping Modulus is defined as:

$$\overline{\mu} = \frac{\mu L^{2}}{\sqrt{\rho A E I}} \tag{42}$$

Normalized Curvature which relates the curvature at any point to the curvature at the middle of the column is defined as:

$$\overline{\kappa} = \kappa / (w_{0,xx})\big|_{x=L/2} \tag{43}$$

Non-dimensional Deflection is defined as:

$$\overline{w} = w / h \tag{44}$$

Non-dimensional Imperfection is defined as:

$$\overline{w}_0 = w_0 / L \tag{45}$$

Slenderness is defined as:

$$s = L / h \tag{46}$$

In this study, all the numerical results were obtained for E = 70 GPa and ρ = 2700 kg/m^3. The geometrical imperfection $w_0(x)$ was chosen as:

$$w_0(x) = W_0 \left[\sin \frac{\pi x}{L} \right]^m \tag{47}$$

where W_0 is the imperfection amplitude, m = 1 for simply supported column and m = 2 for clamped column. The pulse load is chosen as:

$$N_0(t) = \begin{cases} N_0 \sin\left(\frac{\pi t}{T}\right), 0 \le t \le T \\ 0 \qquad\qquad , t \ge T \end{cases} \tag{48}$$

This forcing function allows for a gradual increase in load with time thereby making it easier to achieve numerical stability, as also to simulate the entire spectrum of loads (from impulsive to quasi-static).

CHAPTER III

GEOMETRICALLY PERFECT BEAMS UNDER AXIAL COMPRESSIVE PULSE

It has been shown by Ari-Gur et al (1982) that buckling under dynamic pulse is highly sensitive to the beam imperfection, unlike buckling under static loading. Further, theoretically, a perfectly straight beam can never buckle under a dynamic pulse and it behaves like a rod. Mathematically, there is no singularity or bifurcation that occurs at any point. Therefore the program developed for analysis of beams can be used to analyze rods just by setting beam imperfection to zero.

Convergence

A column with L/h = 100, and $W_0 = 0$ was subjected to a short duration pulse with $T^* = 0.8$ (i.e. 0.157mSec) and load ratio of 100. The maximum axial displacement (Umax) of the loaded end was noted for increasing number of elements (N) starting from N = 10. A plot of percent difference of maximum displacement (of the loaded end) from the maximum displacement with 50 segments versus the number of segments for $\overline{\mu}$ of 0 and 1000, is shown in Figures 4 and 5. From these figures it is evident that sufficient convergence is achieved for N = 50. Therefore N = 50 was chosen for all further analyses.

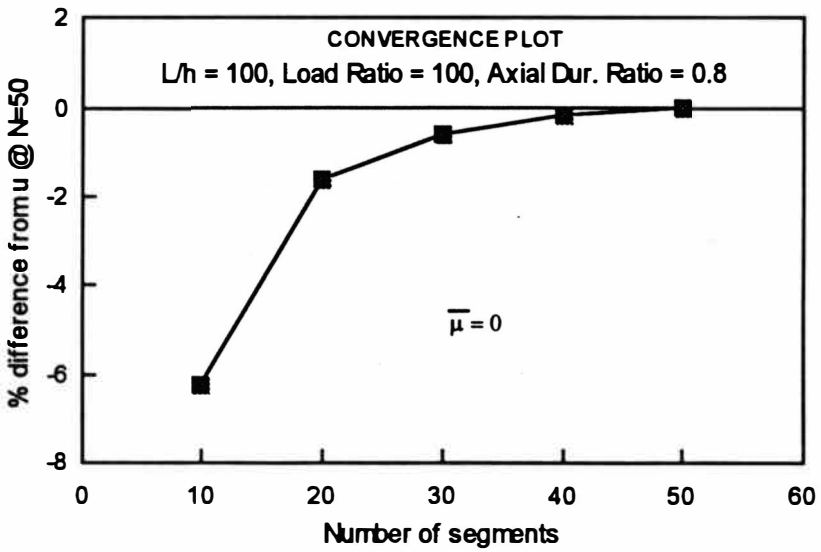

Figure 4. Convergence Plot for Zero Damping.

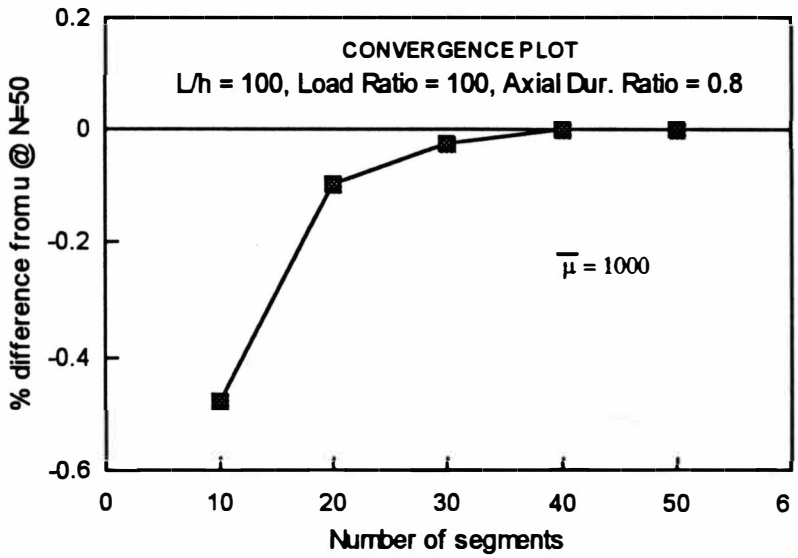

Figure 5. Convergence Plot for High Damping.

Correlation Between $\overline{\mu}$ and Damping Ratio

The ratio between the actual damping modulus to the critical damping modulus (i.e. the limiting value of damping for which the response changes from oscillatory to non-oscillatory) is called the damping ratio(ζ). It is noted that for viscous damping the ratio of successive amplitudes for free vibration is equal to $e^{-2\pi\zeta}$.

A short duration low intensity pulse with $\overline{N}$ = 0.1 (5757N/m) and T^* = 0.1 (i.e. 0.0000196 seconds) was applied to the rod to simulate excitation of free vibration. Successive amplitudes and the corresponding times were plotted, as in Figures (6)-(9), for different values of $\overline{\mu}$. The value of ζ were calculated for each of these cases. A correlation between $\overline{\mu}$ and ζ (%) is shown in Figure 10. It shows that practical damping ratios of up to 5% correlate to $\overline{\mu} \leq 650$.

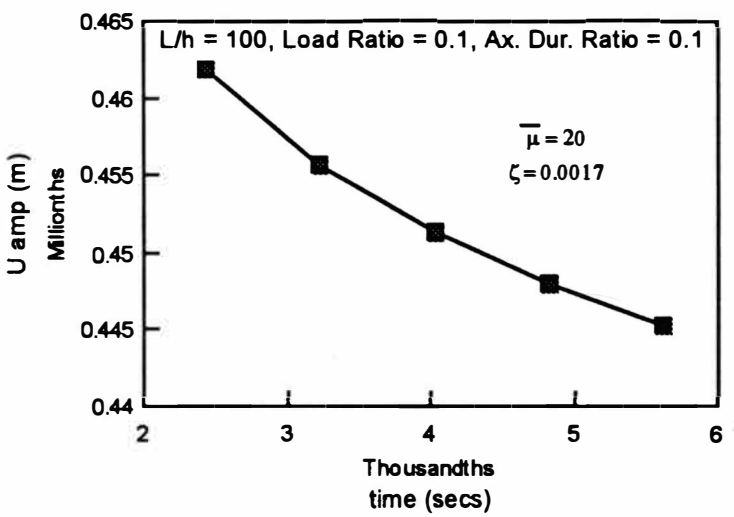

Figure 6. Plot of Successive Amplitudes for $\overline{\mu} = 20$.

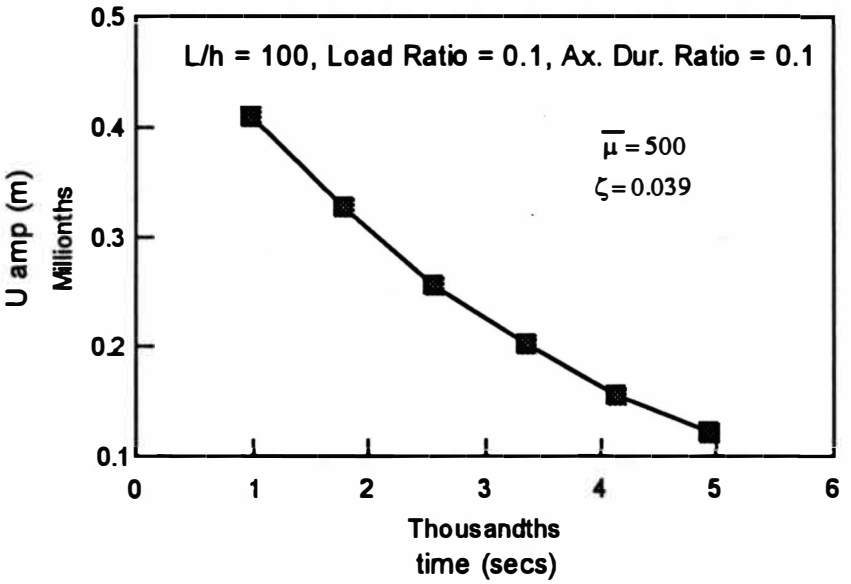

Figure 7. Plot of Successive Amplitudes for $\overline{\mu} = 500$.

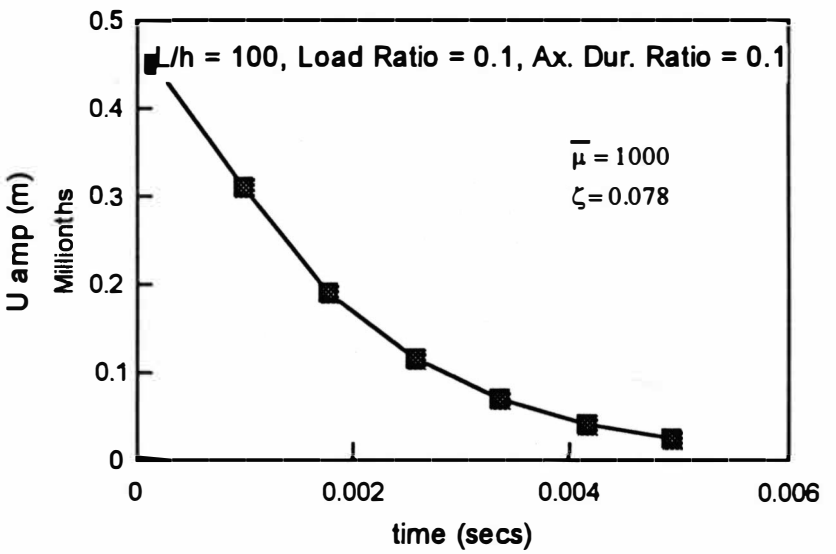

Figure 8. Plot of Successive Amplitudes for $\overline{\mu} = 1000$.

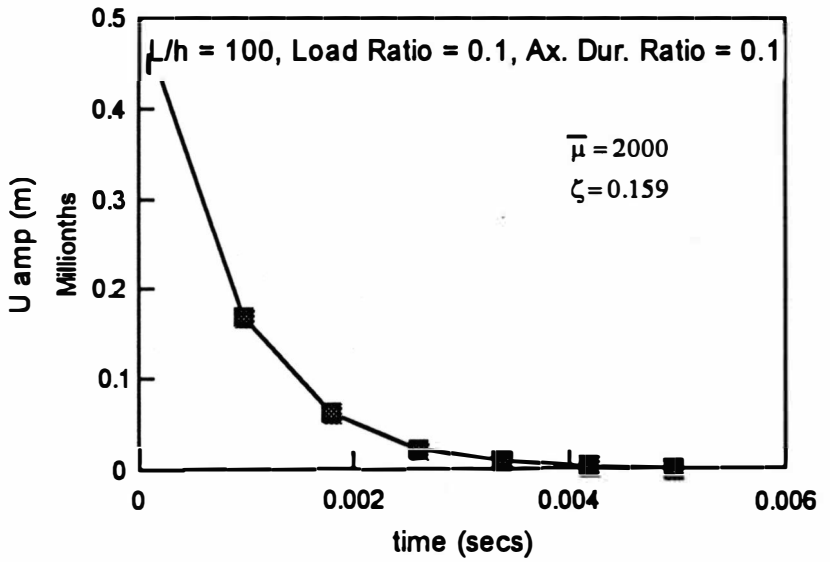

Figure 9. Plot of Successive Amplitudes for $\overline{\mu} = 2000$.

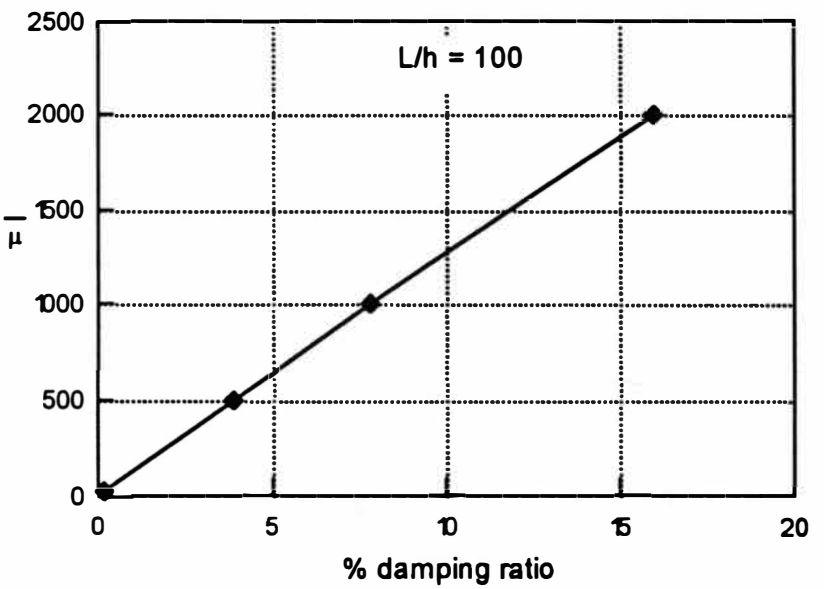

Figure 10. Correlation Between $\overline{\mu}$ and ζ.

Effect of Damping on Forced Vibration of Perfect Columns

A column with L/h = 100 was subjected to a pulse of amplitude equal to its Euler critical load and increasing duration. A plot of the axial duration ratio versus the maximum response, is shown in Figure 11.

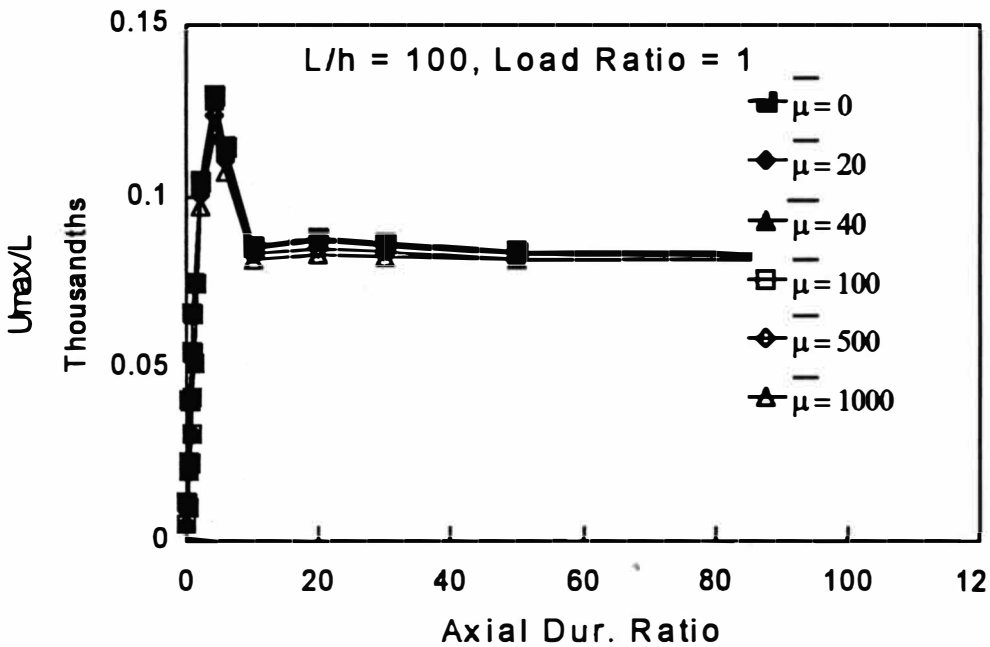

Figure 11. Plot of Maximum Displacement Versus Duration Ratio.

It is evident that damping does not have a significant effect on the maximum displacement of the loaded end of the rod. But, as expected, damping does cause the vibration of the rod to decay rapidly. Regardless of damping the maximum displacement occurs for axial duration ratio of about 4. This may be attributed to the

"resonance effect" that occurs for a duration ratio of about 4. Indeed, a complete cycle of the vibration of the end $x = 0$ occurs during $T^* = 4$.

The peak deflection reaches a steady value for long duration loads. The peak deflection is seen to increase with increase in the pulse duration up to a duration ratio of about 4. $T^* > 10$ is quasi-static.

CHAPTER IV

GEOMETRICALLY IMPERFECT BEAMS UNDER AXIAL COMPRESSIVE PULSE

Convergence

A column with L/h = 100 and Wo/L = 0.0005 was subjected to a pulse with $\overline{N}$ = 69 and $\overline{T}$ = 0.1. Different numbers of elements were tried and Figures 12 and 13 show a plot of the percent difference of peak deflection from the peak deflection with 60 segments versus the number of segments. It can be observed that sufficient convergence is achieved for 60 elements. It can further be observed that increasing the number of elements causes the structure to become stiffer for low damping and less stiff for high damping. Although sufficient convergence was achieved with 40 segments further tests were conducted with 60 elements (unless mentioned) to accommodate smaller wavelengths that could be generated with extremely short duration high intensity pulses. The time step was chosen for numerical stability as discussed in Chapter III. It was observed that once numerical stability was achieved with a particular size of the time interval, decreasing it further did not appreciably alter the solution. Therefore, a separate convergence study based on time interval was not required.

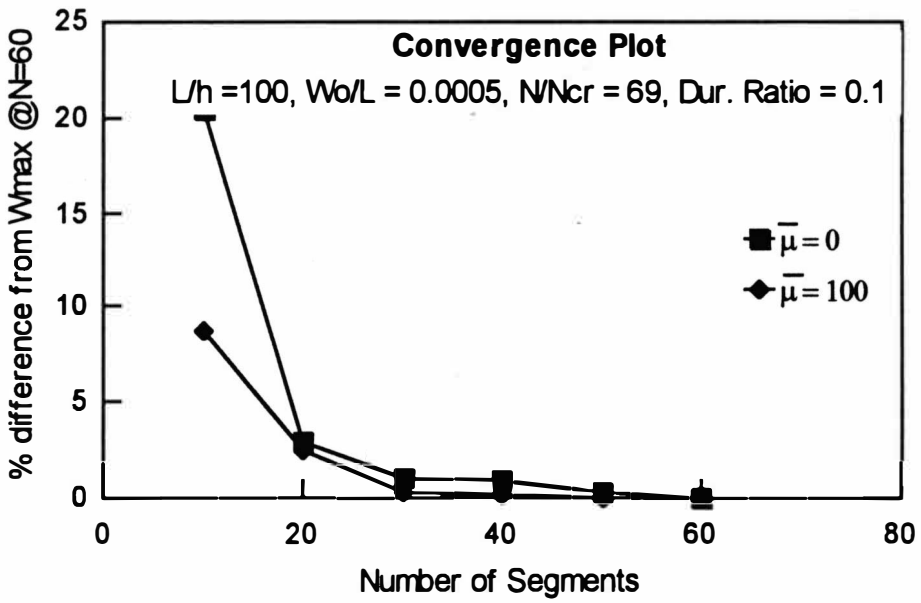

Figure 12. Convergence Plot for Low Damping.

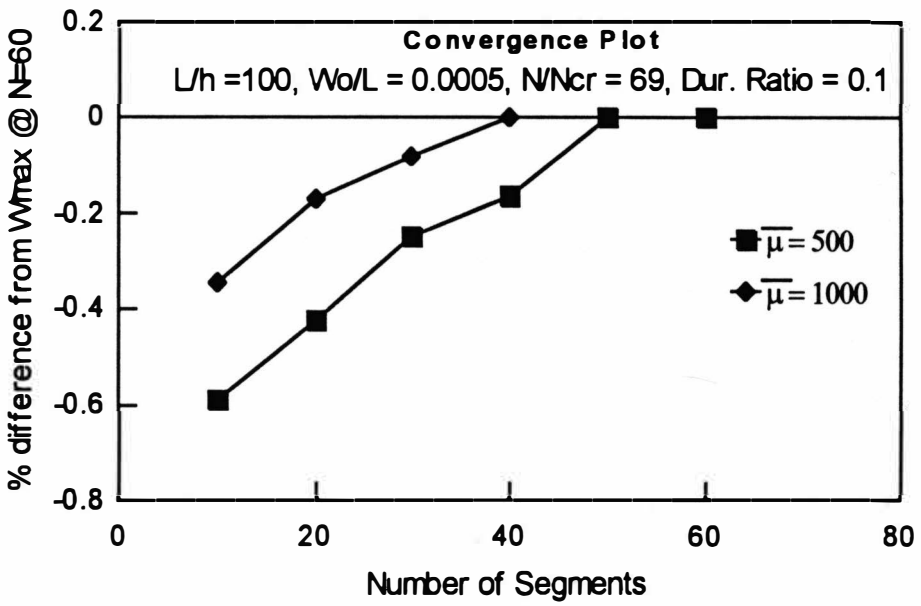

Figure 13. Convergence Plot for High Damping.

Verification of the Program

It is generally accepted that for long duration pulses the response of a column changes from a bounded one to an unbounded one as the pulse intensity approaches the Euler static critical load (i.e. $\overline{N} = 1$). It was therefore sought to test the program for a duration ratio of 10 (quasi-static range) and for increasing load intensities. The column properties were L/h = 100, Wo/L = 0.0005. The maximum deflections were plotted against load intensities. As is evident from the Figure 14 the maximum deflection suddenly increased near a load intensity equal to the Euler critical load. This suggests that the program is a valid tool to investigate this problem. For impulsive loading the results correlated well with those of Ari-Gur et al (1982).

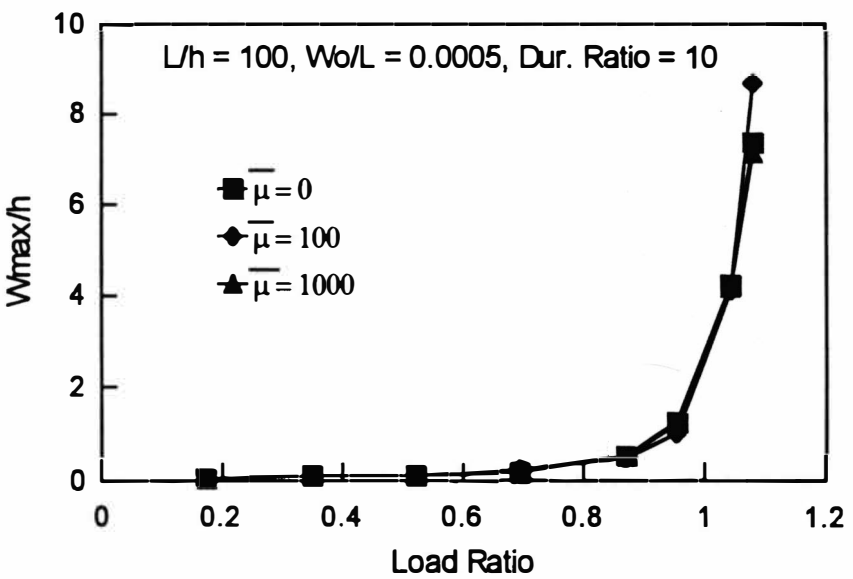

Figure 14. Verification of the Program for a Quasi-Static Pulse.

Pulse Buckling of Columns

Dynamic Buckling Criterion

The buckling criterion that relates the peak lateral deflection (w_{max}) to the intensity of the applied pulse force was initially applied in this study. According to this criterion the limiting load, beyond which a small increase of intensity will cause a relatively large increase in the deflection, was defined as the "Dynamic Buckling load". This resembles the Budiansky-Hutchinson (1964) dynamic buckling criterion, according to which buckling occurs when a small increase in load intensity causes a transition from a bounded response to an unbounded one. Figures 15 and 16 show plots of load ratio versus maximum deflection, for duration ratios of 1.0 and 0.1. It can be inferred that this criterion can provide satisfactory results for quasi-static to dynamic loads. However for impulsive (duration ratio of 0.1) loading the plot of w_{max} does not suggest a conclusive trend. An investigation of the shape of the column under short pulses revealed short wavelengths. Therefore, it was concluded that increasing the load intensity does not necessarily cause an increase in the value of peak deflection, especially for short pulses. Due to this fact it appears as though the stiffness of the beam is varying (increasing as well as decreasing) as the load intensities increase, whereas buckling is marked by a sudden fall of stiffness. Recognizing this, curvature was chosen as a more appropriate variable. An increase in the number of wavelengths obviously implies an increase in the curvature ($w_{,xx}$). Figures 17 and 18

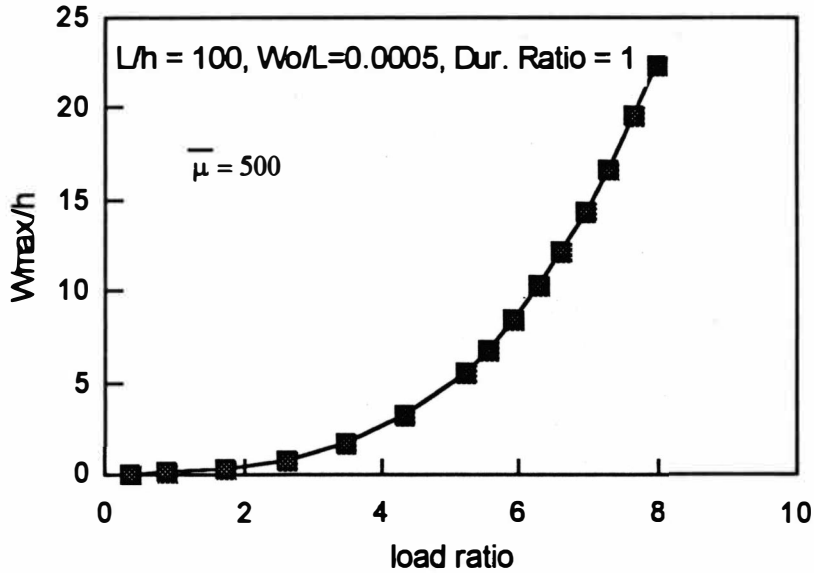

Figure 15. Peak Deflection Versus Load Ratio for a Dynamic Range Pulse.

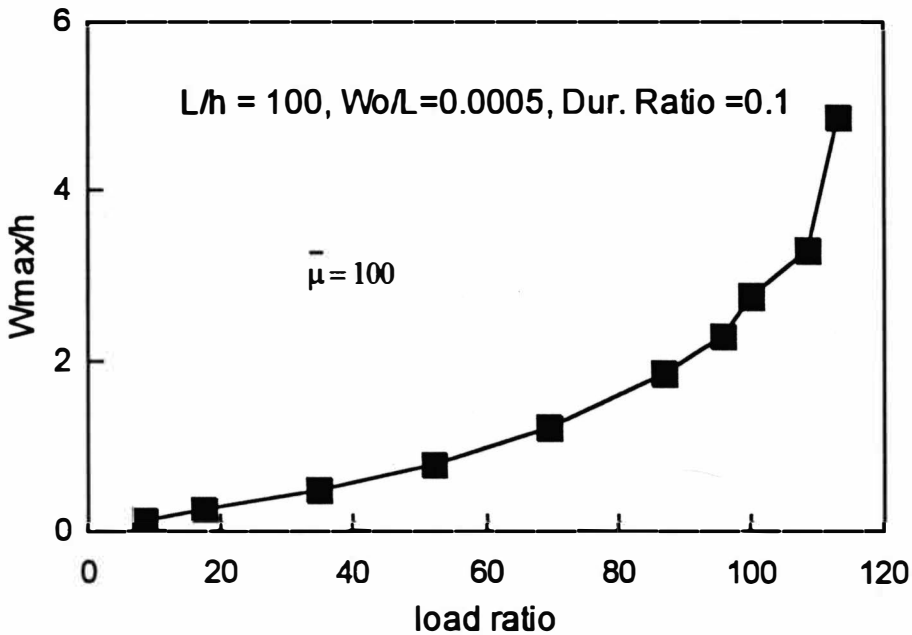

Figure 16. Peak Deflection Versus Load Ratio for Impulsive Pulse.

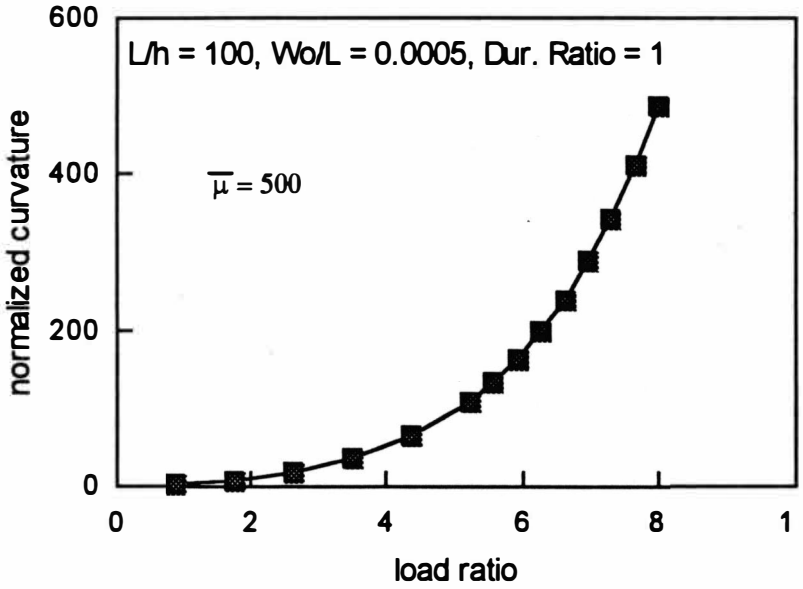

Figure 17. Peak Curvature Versus Load Ratio for a Dynamic pulse.

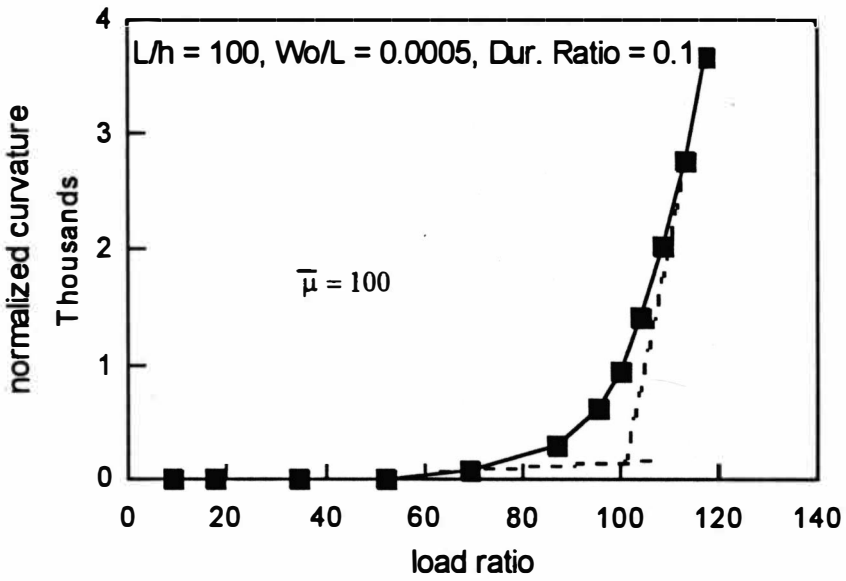

Figure 18. Peak Curvature Versus Load Ratio for an Impulsive Pulse.

show the normalized curvature plots. It can be seen that these plots provide a very conclusive trend.

A more appropriate variable would seem to be the peak root mean square of the curvature. But this variable did not prove to improve the quality of results within the scope of this study. Therefore it was decided to conduct all further tests based on peak curvature.

Buckling was defined when a small increase in pulse intensity resulted in a relatively large increase in the peak curvature. This criterion is henceforth called the "curvature criterion" in this report. The buckling load, according to this criterion, may be determined by finding the point of intersection of the two dominating slopes in the trend as shown in Figure 18.

A less "subjective" approach is to obtain the upperbound of the dynamic response from the Southwell plot, based on the curvature versus the pulse intensity plot. Figure 19 shows one such plot. This plot is based on the results of in Figure 18. This criterion is henceforth called the " Southwell Curvature Criterion" in this report. Obviously this criterion will yield a higher load as compared to the curvature criterion (because this gives the upper bound).

The buckling load obtained from either criterion is normalized relative to the Euler critical load and defined as the "Dynamic Load Factor-Curvature" (DLF-C) and "Dynamic Load Factor-Southwell" (DLF-S) as the case may be.

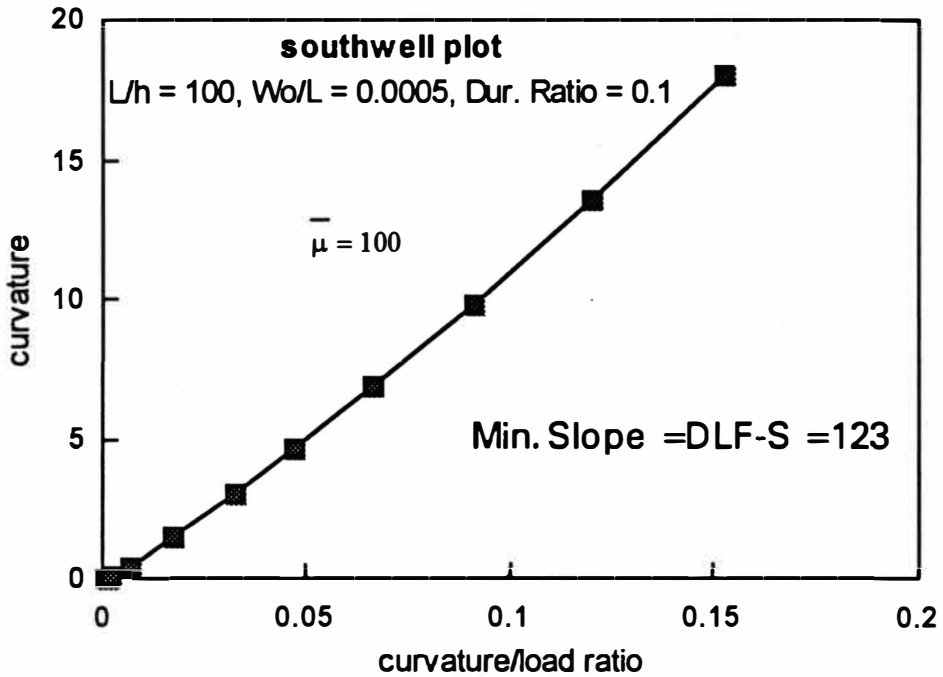

Figure 19. Southwell Plot Based on Figure 18.

Effect of Load Duration on Pulse Buckling

In this section the effect of load duration on buckling is studied. The load intensity was steadily increased for various durations ranging from quasi-static to impulsive. All the runs in this section were conducted for a normalized damping modulus of 20 (i.e. damping ratio of 0.16%) and for simply supported end conditions.

Figure 20 shows the plot of maximum deflection versus the load for various duration ratios ranging from $\bar{T} = 10$ to $\bar{T} = 0.1$. It can be concluded that as the load duration decreases the column can endure higher load intensities before buckling. It can be observed that for comparable load intensities shorter durations cause smaller

peak deflections. It can further be observed that the plot is not very conclusive for very short duration pulses (e.g. $\overline{T} = 0.1$). This can be explained by observing Figure 21, which shows the shape of the column when maximum deflection occurs for a duration ratio of $\overline{T} = 0.1$ and various intensities. It can be observed that as the load intensity is increased from load ratio 70 to 110 smaller wavelengths are generated. This implies that much of the applied energy goes into increasing the curvature under high intensity impulsive loads.

Figure 22 shows the plot of the peak normalized curvature versus the load ratio. Comparing the trends for duration ratios of 0.1 and 0.2 in Figure 20 and 22, it can be observed that the plot of curvature exhibits a "sharper" transition to the region of lower stiffness.

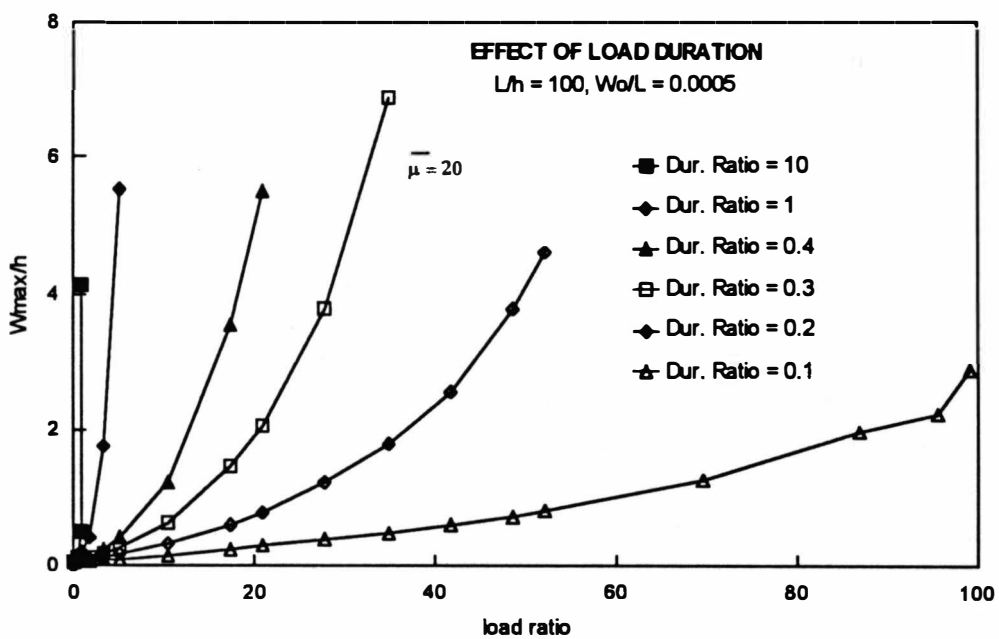

Figure 20. Normalized Peak Deflection Versus Load Ratio.

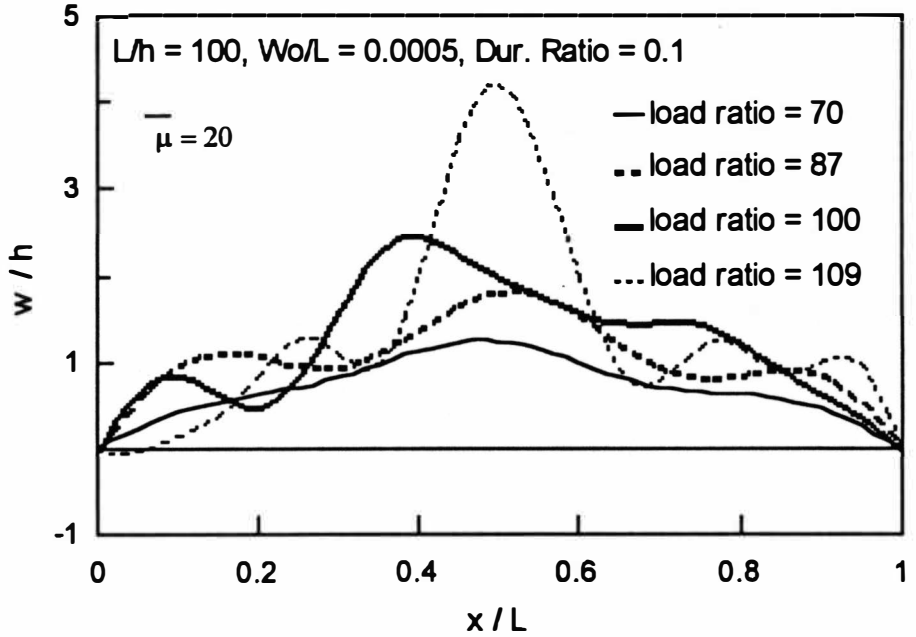

Figure 21. Shape of the Column When Peak Deflection Occurs for Increasing Loads.

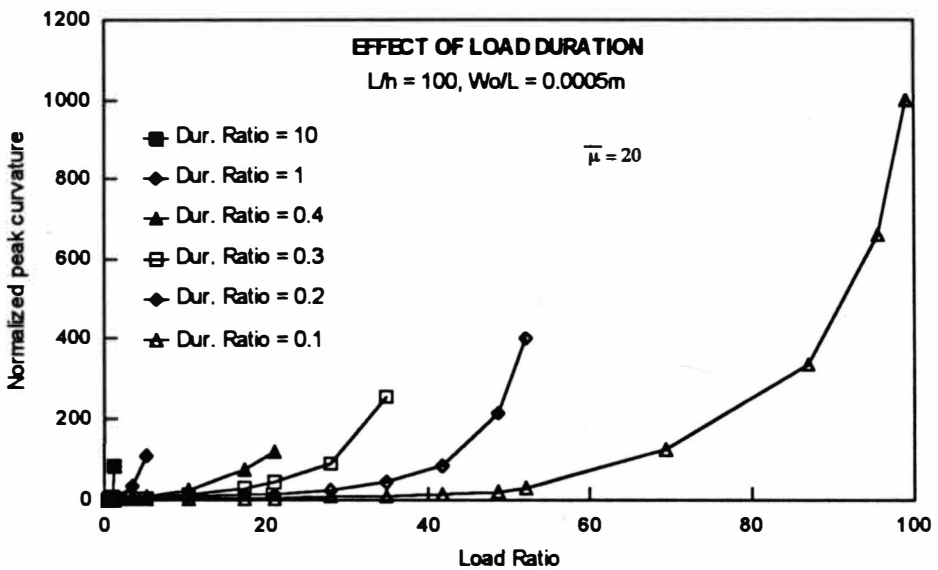

Figure 22. Peak Normalized Curvature Versus the Load Ratio.

The non-dimensional buckling load (DLF-C) was determined for duration ratios of 0.05, 0.2 and 1.0. The shape of the column when the maximum curvature occurs is presented in Figure 23. It is evident that under impulsive loading the column buckles into shorter wavelengths.

Figure 24 shows the plot of DLF-C against the duration ratio. DLF-C was 170 for duration ratio of 0.05 and close to unity for a duration ratio of 10. It can be concluded that as $\overline{T} \to 0, DLF - C \to \infty$ and as $\overline{T} \to \infty, DLF - C \to 1$. A major change of slope occurs at a duration ratio between 0.4 and 1.0.

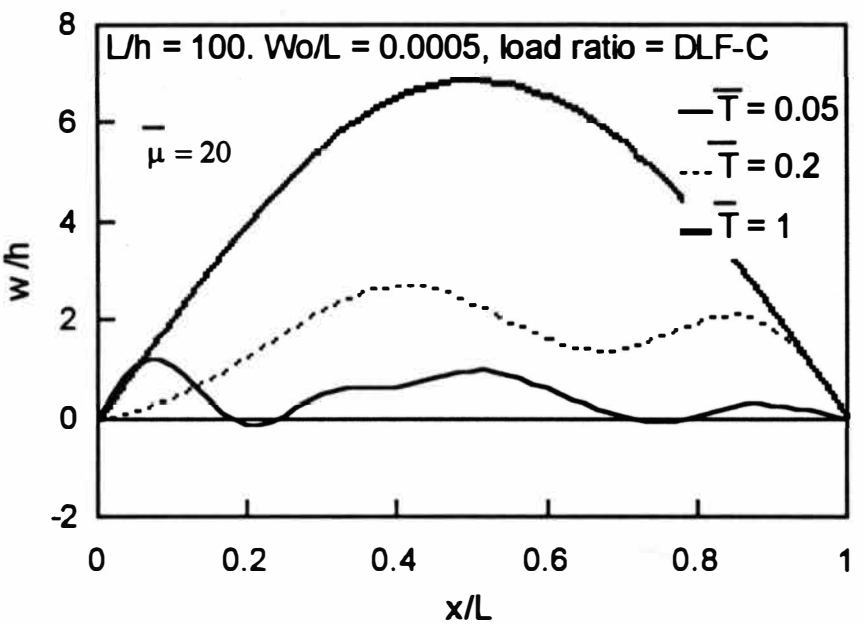

Figure 23. Shape of the Buckled Column for Various Load Durations.

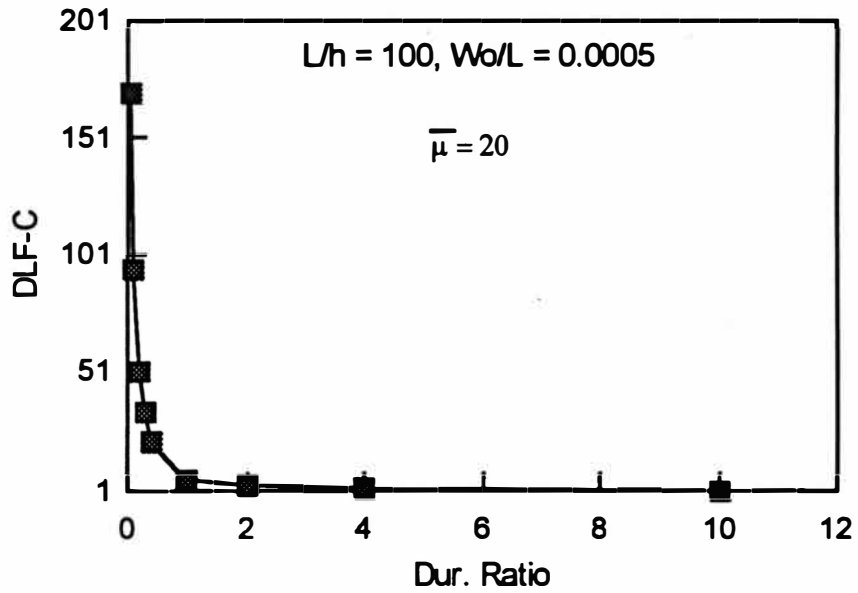

Figure 24. Effect of Load Duration on Dynamic Buckling Load.

Effect of Viscous Damping on Pulse Buckling

As stated before a Voigt-Kelvin constitutive equation was used in this study. A correlation between the viscous damping modulus (μ) and the damping ratio (ζ) is presented in Chapter III. It was observed that smaller time steps were required when the damping values were large for stability of the routine. At the same time it was observed that fewer elements were enough to achieve convergence for larger damping values. Hence, this study has been restricted to values of $\overline{\mu}$ up to 2000.

The dynamic response of the column was studied for various pulse duration and viscous damping values. Figures 25 - 31 show plots of the peak deflection versus load ratio for various values of viscous damping.

For relatively long duration loads (e.g. $\overline{T} = 10$) there are two distinct regions in the plot, i.e. one in which the slope is moderate and the other in which a small increase in load causes a large increase in deflection. It can be observed that for short load durations this trend becomes less conclusive. It can be further observed that, as anticipated, viscous damping plays a very insignificant role in case of long duration pulses. However for short pulses it can be inferred from these plots that the load carrying capacity of the column increases for higher values of viscous damping. Figures 32-38 show the corresponding plots of load ratio versus peak curvature.

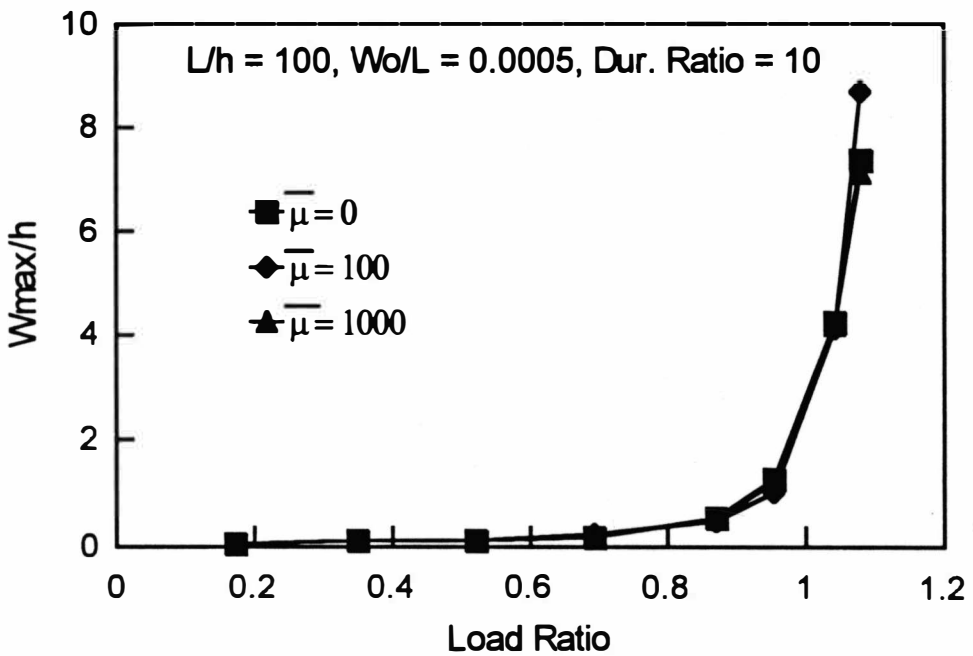

Figure 25. Normalized Peak Deflection Versus Load Ratio ($\overline{T} = 10$).

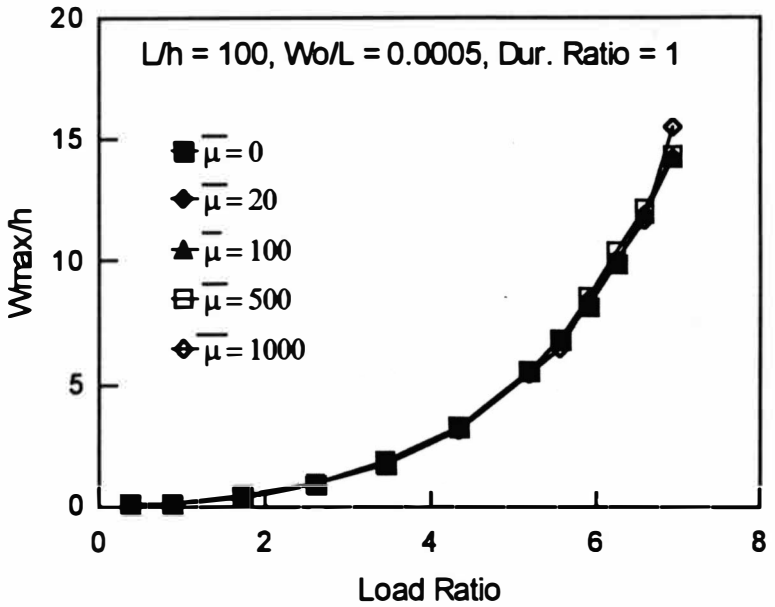

Figure 26. Normalized Peak Deflection Versus Load Ratio ($\overline{T}$ = 1).

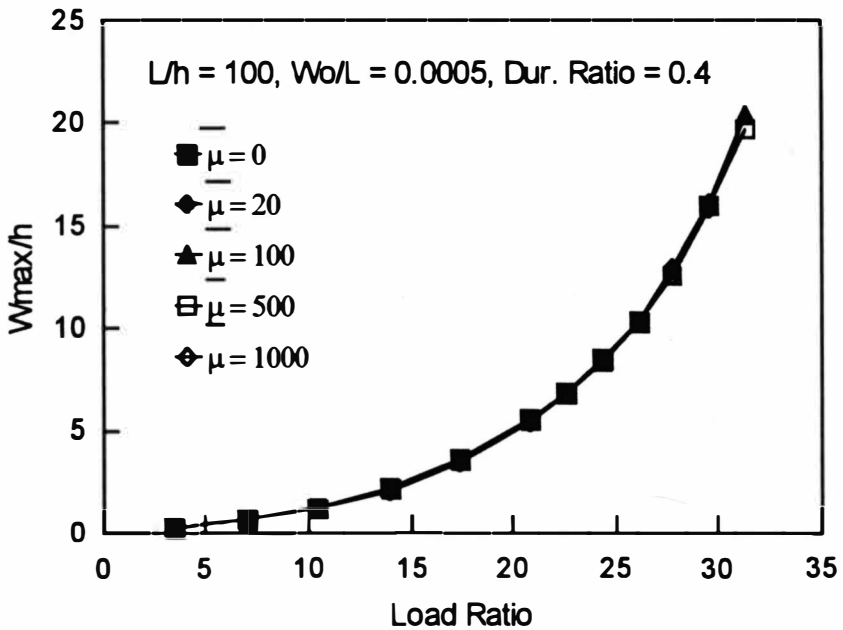

Figure 27. Normalized Peak Deflection Versus Load Ratio ($\overline{T}$ = 0.4).

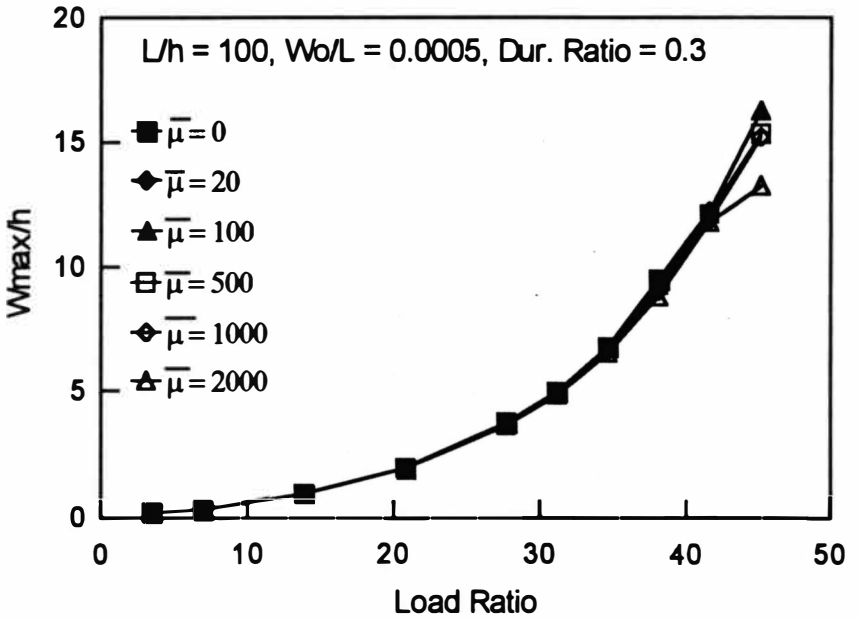

Figure 28. Normalized Peak Deflection Versus Load Ratio ($\overline{T}$ = 0.3).

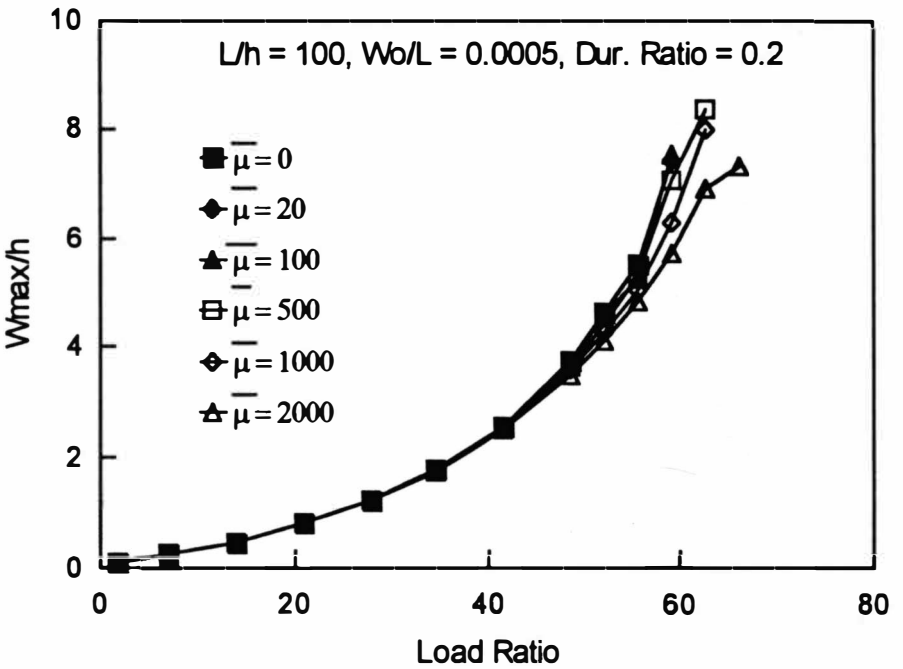

Figure 29. Normalized Peak Deflection Versus Load Ratio ($\overline{T}$ = 0.2).

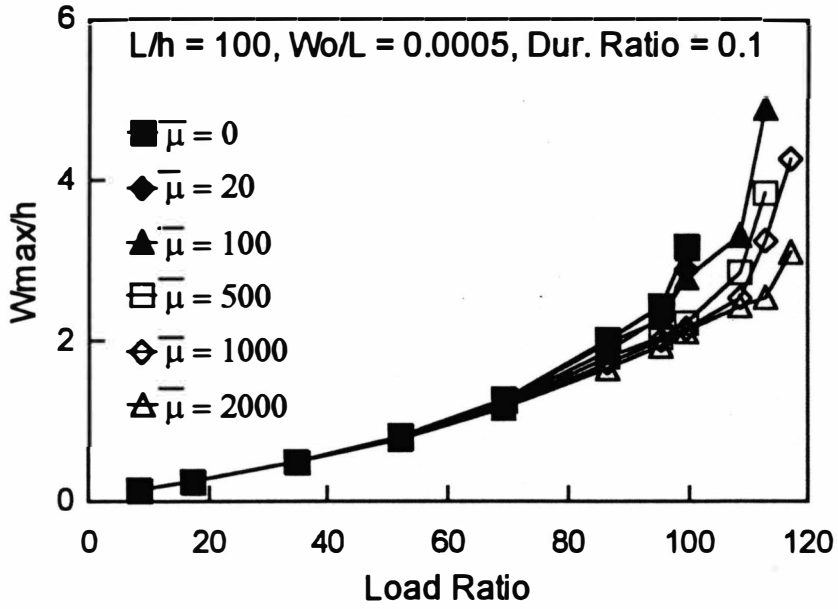

Figure 30. Normalized Peak Deflection Versus Load Ratio ($\overline{T}$ = 0.1).

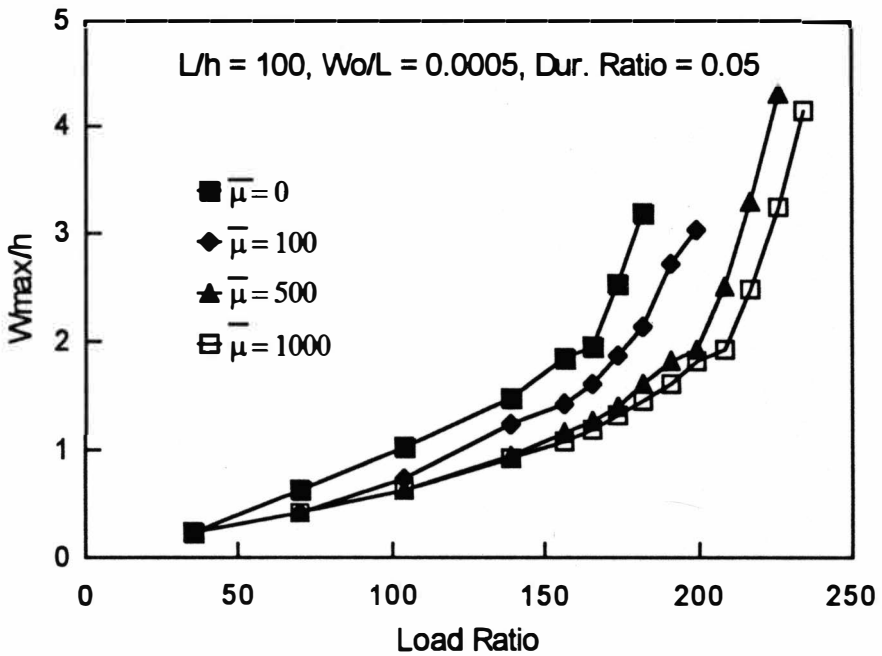

Figure 31. Normalized Peak Deflection Versus Load Ratio ($\overline{T}$ = 0.05).

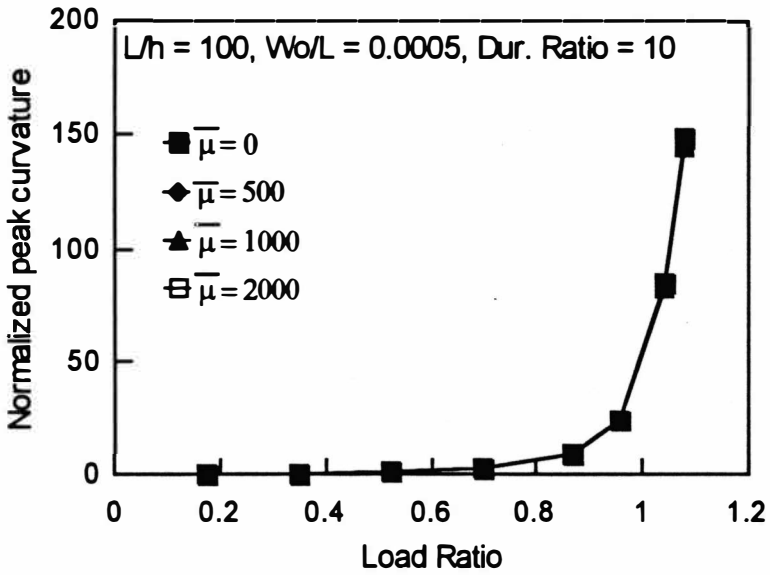

Figure 32. Normalized Peak Curvature Versus Load Ratio ($\overline{T}$ = 10).

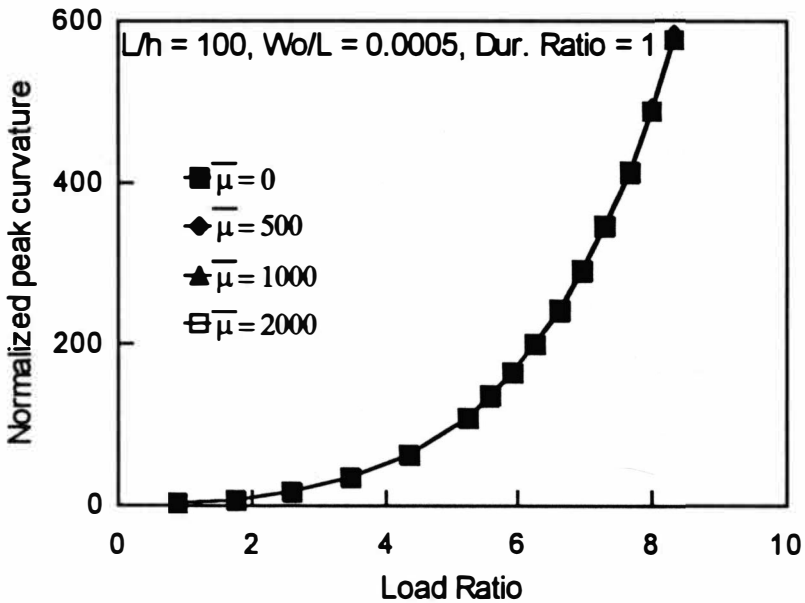

Figure 33. Normalized Peak Curvature Versus Load Ratio ($\overline{T}$ = 1).

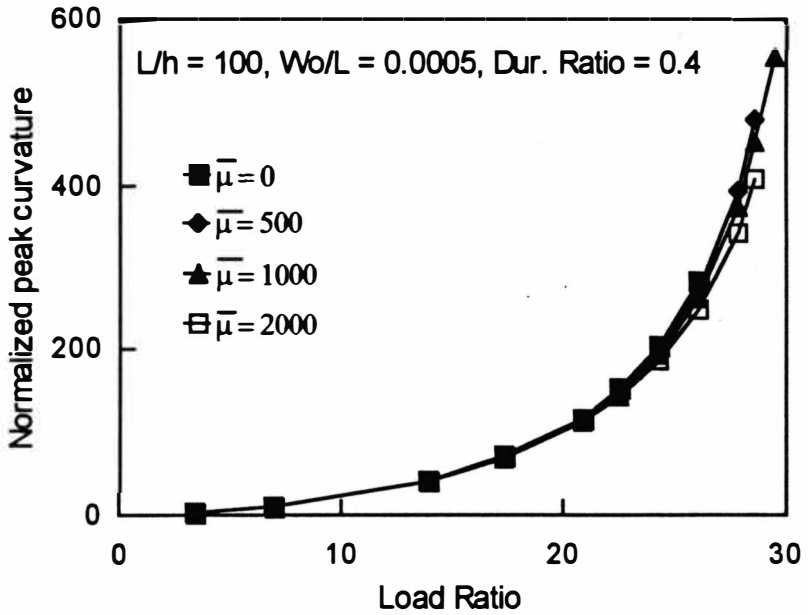

Figure 34. Normalized Peak Curvature Versus Load Ratio ($\overline{T}$ = 0.4)

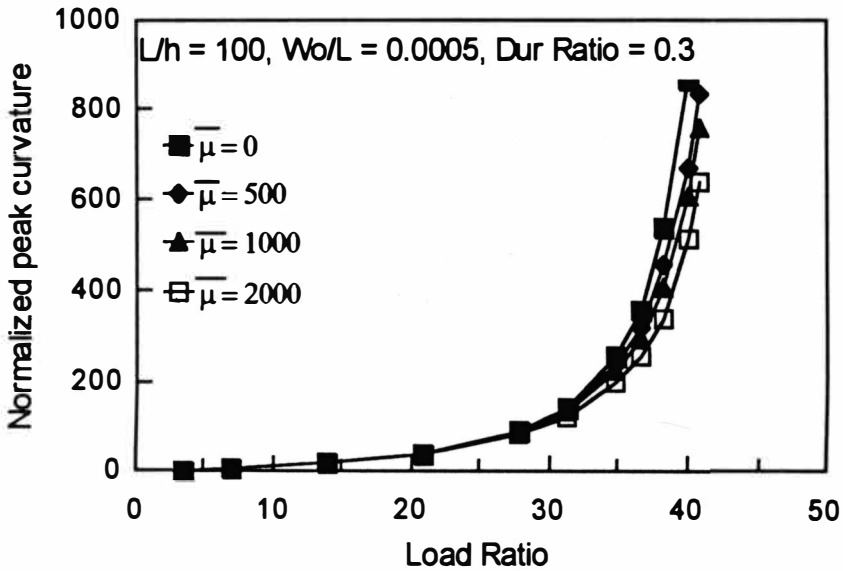

Figure 35. Normalized Peak Curvature Versus Load Ratio ($\overline{T}$ = 0.3).

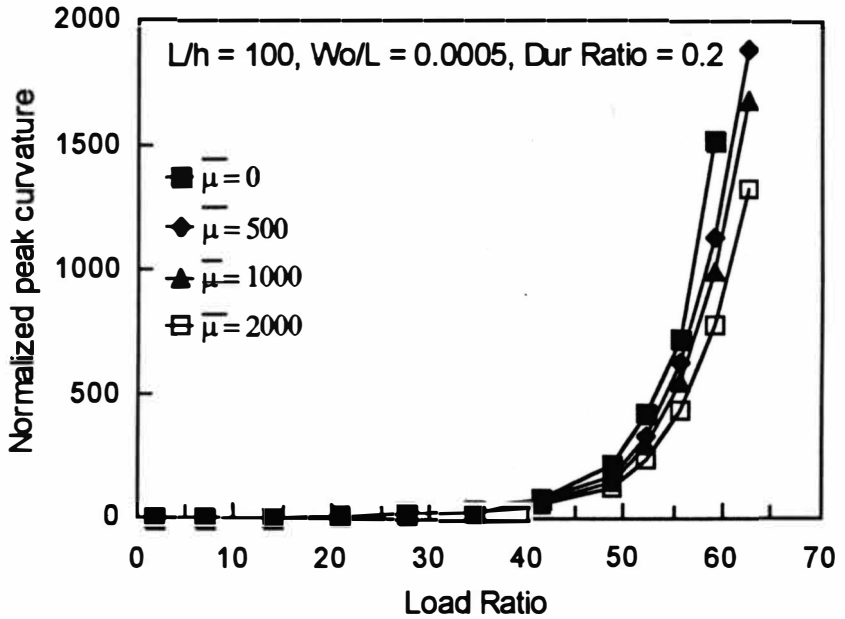

Figure 36. Normalized Peak Curvature Versus Load Ratio ($\overline{T}$ = 0.2).

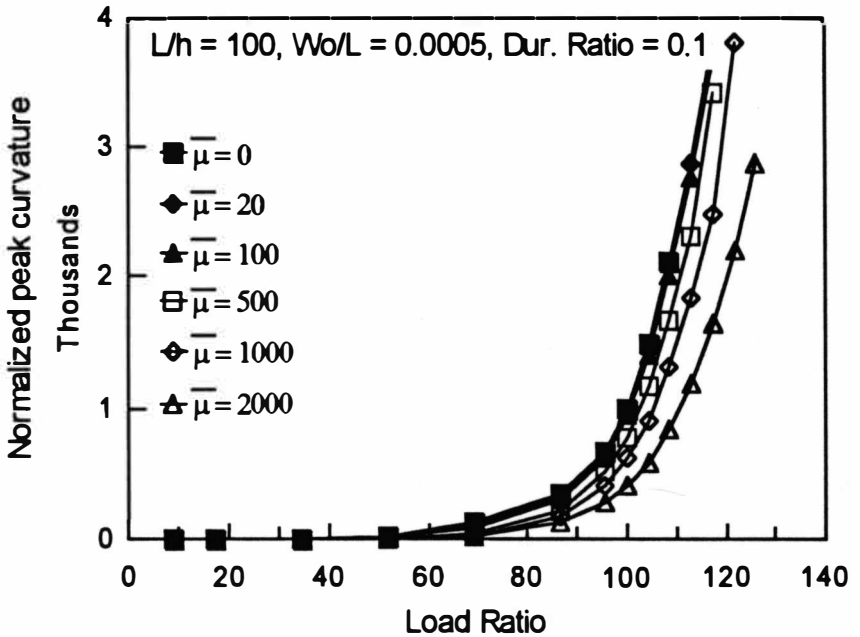

Figure 37. Normalized Peak Curvature Versus Load Ratio ($\overline{T}$ = 0.1).

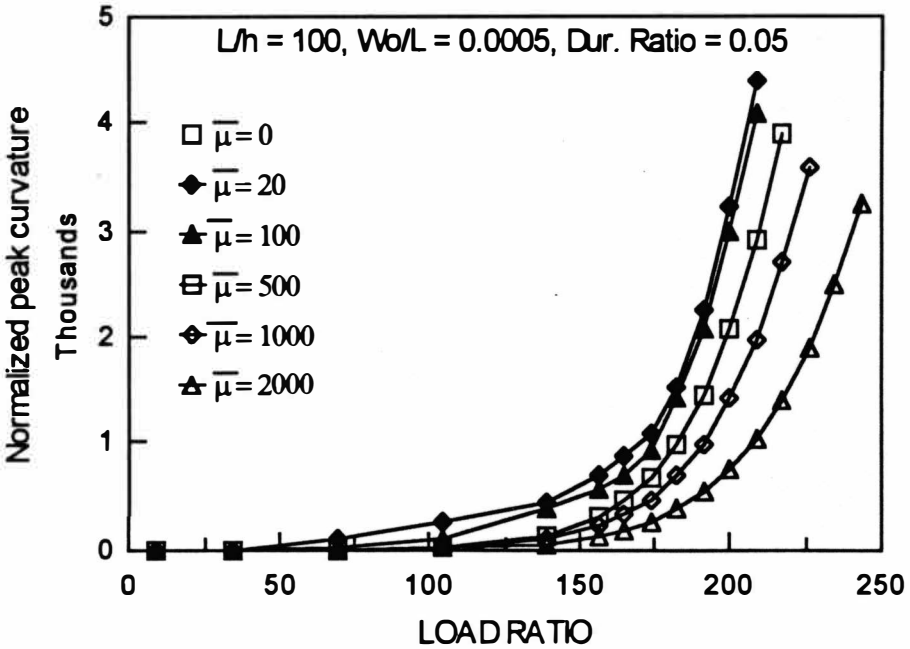

Figure 38. Normalized Peak Curvature Versus Load Ratio ($\overline{T}$ = 0.05).

It can be observed that these plots provide a more consistent trend (i.e. two distinct regions in the plot) as compared with the peak deflection plots. The effect of viscous damping becomes evident for duration ratios of less than 0.4 but it is insignificant under relatively long pulses. Figure 39 shows the plot of increase in the DLF-C versus the non-dimensional damping modulus. It can be observed that for $\overline{T}$ = 0.05 and $\overline{\mu}$ = 2000, the DLF is about 20% greater than that for $\overline{\mu}$ = 0.

Figure 40 shows the shape of the deflected beam when the peak deflection occurs, under similar impulsive loading conditions. The presented results are for $\overline{T}$ = 0.1 and $\overline{N}$ = 87.

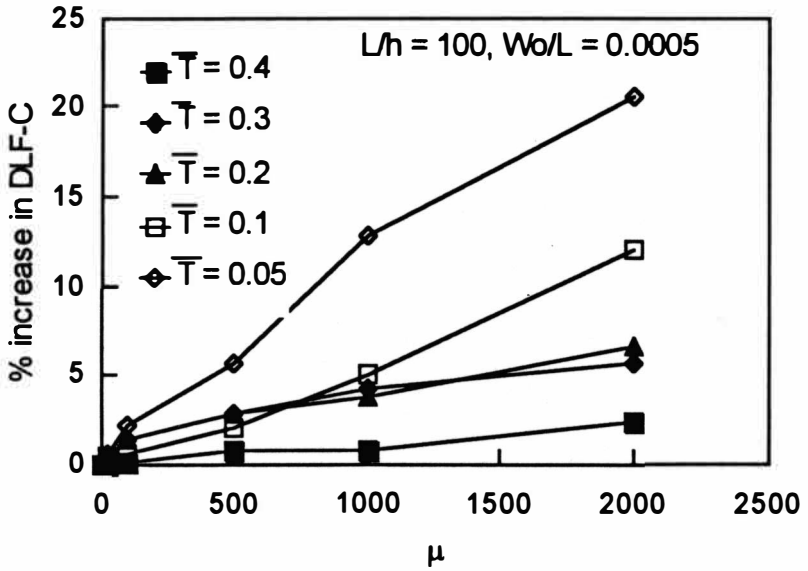

Figure 39. The Effect of Viscous Damping on DLF.

It can be observed that the deflection pattern "smoothens" as the damping increases. This is attributed to the coupling of modes and the transfer of energy from higher modes to lower modes. Numerically this (lowering of curvature for large viscous damping) resulted in a smaller number of elements required to achieve convergence.

It was observed that for long duration loads the time for maximum deflection very closely matched the time for maximum curvature. However, for short pulses the peak curvature and deflection occurred at significantly different times. In either case higher viscous damping caused the peaks to occur early.

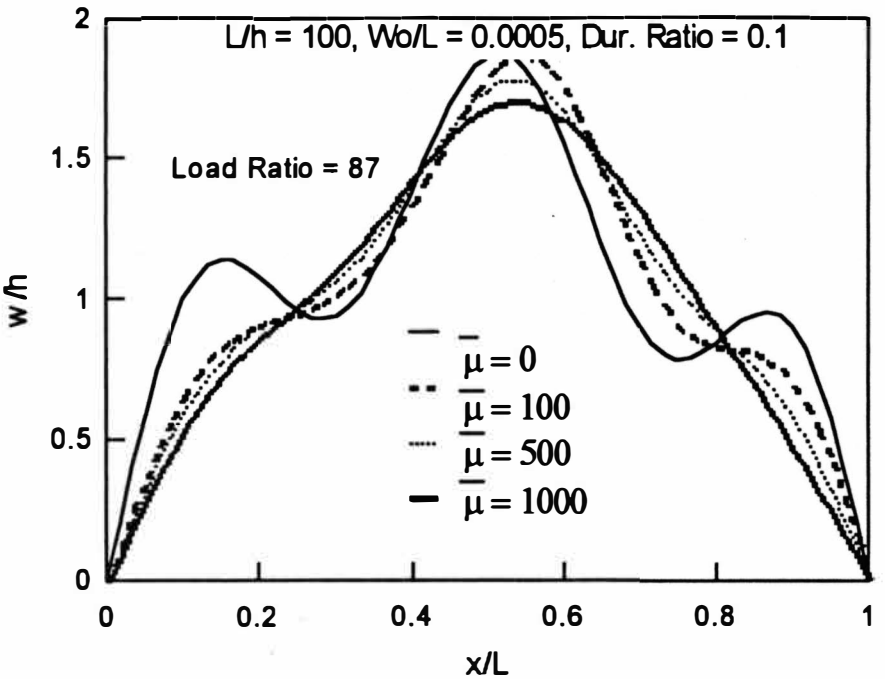

Figure 40. Effect of Viscous Damping on the Deflection Pattern.

Effect of Rotary Inertia on Pulse Buckling

Rotary inertia signifies the resistance of the column to dynamic bending. It can be assumed to be particularly significant during wave propagation and when the deflection pattern involves shorter wavelengths. Furthermore, from previous analysis it can be assumed to be more significant for short and intense pulses because they tend to result in shorter wavelengths.

Figures 41 and 42 show the plot of the load ratio versus the normalized peak curvature for a pulse of duration ratio of 0.2 and a column with L/h ratio of 66.66 and

200, respectively. It can be observed that including rotary inertia in the analysis of slender columns does not significantly affect the results.

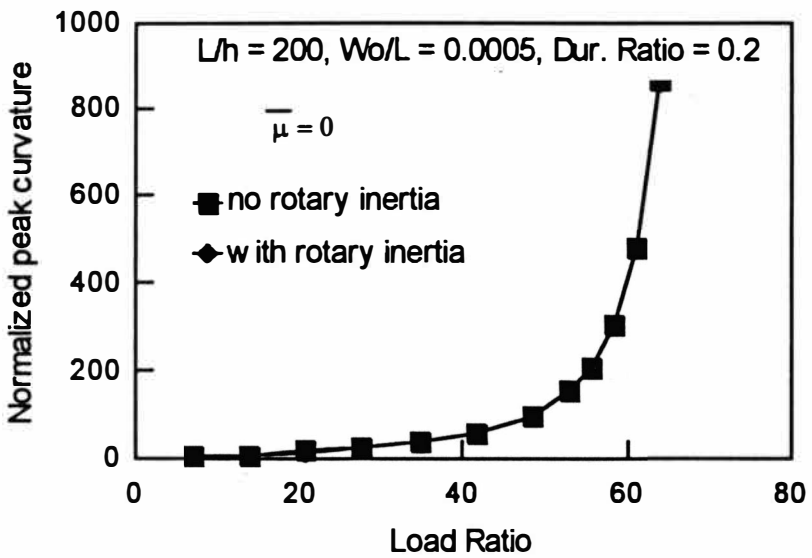

Figure 41. Effect of Rotary Inertia on Buckling (L/h = 200).

Figure 43 illustrates the shape of the buckled column with L/h = 100. Results with and without inclusion of rotary inertia terms are presented for a duration ratio of 0.2 and load equivalent to DLF-C. This suggests that rotary inertia does not affect the shape of the buckled column either. Therefore rotary inertia may be neglected from the analysis of thin columns to reduce the computational effort. Since the inertia moment is proportional to cube of the column thickness it may be significant in case of thicker columns. Within the scope of this study (L/h > 66.66) rotary inertia is insignificant.

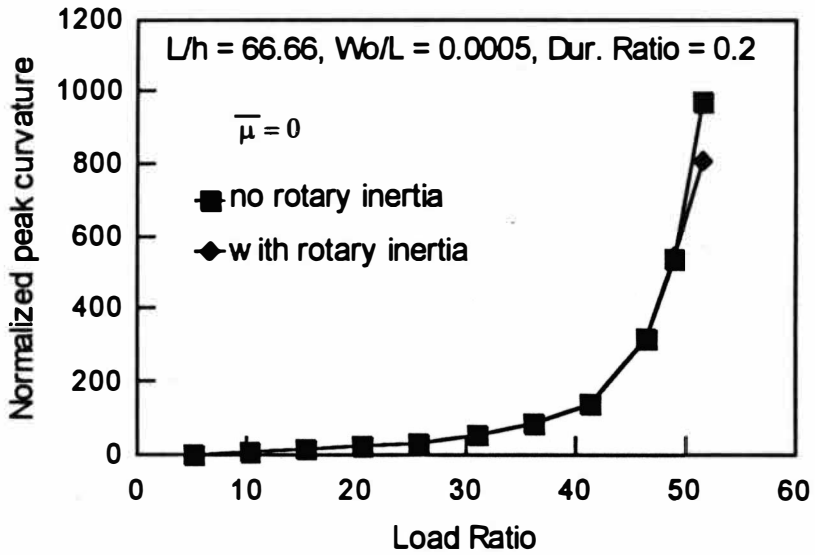

Figure 42. Effect of Rotary Inertia on Buckling (L/h = 66.66).

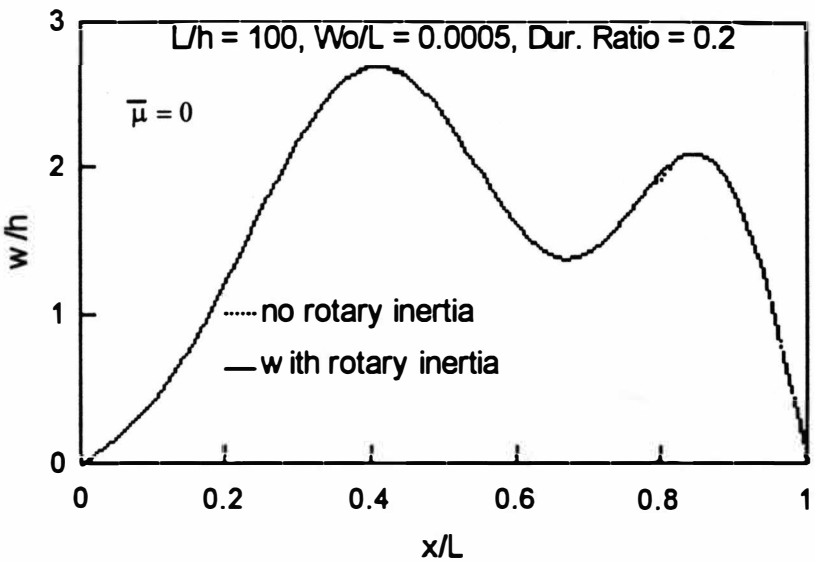

Figure 43. Effect of Rotary Inertia on Shape of the Column (L/h = 100).

Effect of Imperfection Size on Pulse Buckling

Different amplitudes of initial imperfection were analyzed for impulsive and quasi-static loading. Plots of peak curvature versus load ratio for various initial imperfections are presented in Figures 44 and 45 for duration ratios of 0.05 and 10, respectively. Using the "curvature criterion" in Figure 43 the buckling load is seen to increase for decreasing initial imperfection. In Figure 44 it can be observed that DLF-C for all cases are much closer to each other. It is evident that buckling under impulsive pulses is more sensitive to initial imperfection than buckling under quasi-static pulses.

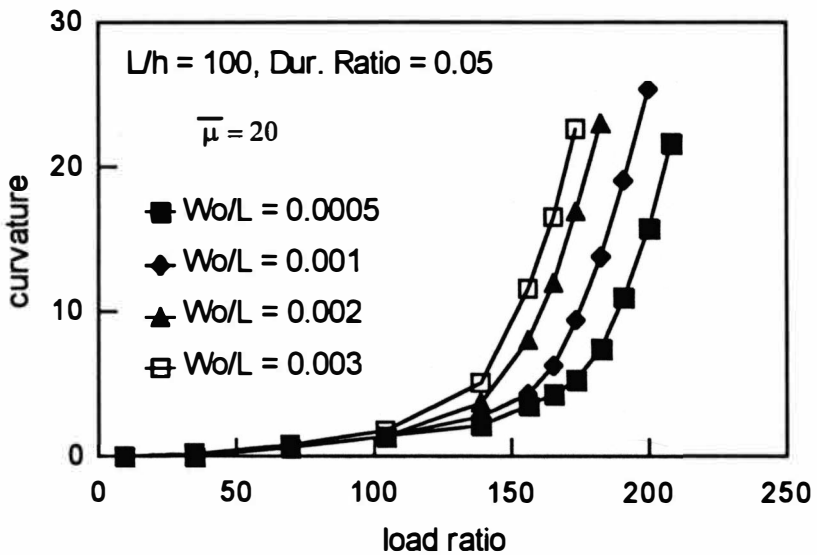

Figure 44. Effect of Initial Imperfection Size (Impulsive Loading).

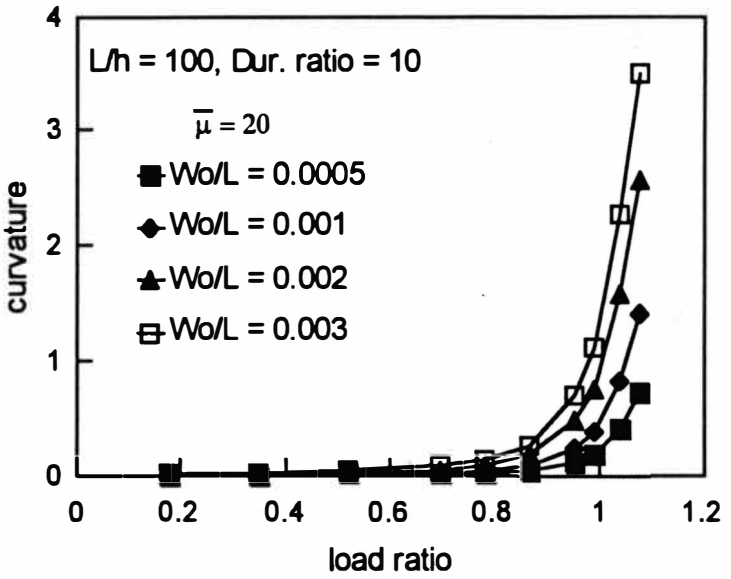

Figure 45. Effect of Initial Imperfection Size (Quasi-Static Loading).

CHAPTER V

CONCLUSION

Dynamic pulse buckling of viscoelastic columns with half sine imperfection was studied. It was seen that for very short pulses the column could bear load intensities much in excess of the static critical load. Viscous damping was seen to have significant effect under pulses of duration ratio less than 0.4 (i.e. very short pulses). The DLF with $\overline{\mu}$ = 2000 was about 20% higher than that without damping for a duration ratio of 0.05.

Within the scope of this study, i.e. slender columns, rotary inertia effects were seen to be insignificant. It was further observed that buckling under quasi-static loading was less sensitive to initial imperfection as compared to that under impulsive loading.

A study of geometrically perfect beams showed that a viscous damping of $\overline{\mu}$ = 2000 correlated with a damping ratio of 16%. Effect of different pulse durations and damping on the peak displacement was studied. Viscous damping was seen to be quite insignificant. The maximum displacement occurred for an axial duration ratio of about 4.

This study gives an insight into the behavior of viscoelastic materials under dynamic pulse loading. The next logical step would be to use a more appropriate

viscoelastic constitutive equation such as the one given by the Boltzman Superposition principle, as:

$$\sigma = E_o \varepsilon + \int_0^t \dot{E}(t - t')\varepsilon dt'$$

where E(t) is the relaxation function, E_0 its value at t = 0.

Another interesting problem that can be analyzed using the same approach is the pulse buckling of viscoelastic plates.

Appendix A

Computer Program for Analysis

```
REM ### PROGRAM FOR DYNAMIC PULSE BUCKLING ANALYSIS ####

CLS
DEFINT I-J, L
DEFDBL A-H, K, M-Z
PI = 4 * ATN(1)

REM ## INPUTS ##

INPUT " INPUT THE ELASTICITY MODULUS,E ="; E
INPUT " INPUT THE DAMPING MODULUS "; V
INPUT " DENSITY "; D
INPUT " COLUMN LENGTH "; OL
INPUT " COLUMN THICKNESS "; H
INPUT "IMPERFECTION AMPLITUDE"; Wm
INPUT " INITIAL IMPERFECTION WAVE # "; M%
INPUT " INPUT THE LOAD DURATION = "; T
INPUT " INPUT THE END OF ANALYSIS = "; TS
INPUT " HOW MANY LOADS TO BE TESTED =?"; I9
DIM N9(I9)
FOR I = 1 TO I9
PRINT " INPUT THE LOAD #"; I; "=?"
INPUT N9(I)
NEXT I
INPUT " INPUT THE # OF SEGMENTS "; IN
INPUT " INPUT THE TIME INTERVAL FACTOR = "; I2
INPUT " IS ROTARY INERTIA SIGNIFICANT (NO = 0/ YES = 1)"; R%
I1 = 1
F = 0

REM ################## CALCULATIONS ########################

C = SQR(E / D)
DX = OL / IN
DT = DX / (I2 * C)
NT& = (TS / DT) + 1
REM * THE NO. OF DATA POINTS ON THE BEAM
IP = IN + 1

DX2 = DX * DX
DT2 = DT * DT

REM ########################################################
```

```
REM * DEFINE ARRAY SIZE
DIM W0(IP), U(IP, 3), W(IP, 3), W01(IP), W012(IP), W02(IP)
DIM EP(IP, 2), KA(IP, 2), EPD(IP), KAD(IP), NX(IP), MX(IP)
DIM RHS(IP), RH(IP), A(IP, IP), P(IP, IP), DA(IP, IP)
DIM RHS1(IP), RHS2(IP), RHS3(IP)
DIM UX(IP), WX(IP, 2), WXX(IP, 2), NXX(IP), MXXX(IP)

REM ##########################################################
REM ##########################################################

FOR J = 2 TO IN
  W0(J) = Wm * SIN(PI * M% * (J - 1) / IN)
NEXT J
W0(IP) = 0: W0(1) = 0
W01(1) = W0(2) / DX: REM # FIRST DERIVATIVE OF W0
W012(1) = W01(1) ^ 2
FOR J = 2 TO IN
  W01(J) = (W0(J + 1) - W0(J - 1)) / (DX * 2)
  W012(J) = W01(J) ^ 2
NEXT J
W01(IP) = -W0(IN) / DX
W012(IP) = W01(IP) ^ 2

REM ## SECOND DERIVATIVE OF INITIAL IMPERFECTION FUNCTION
W02(1) = 0
FOR J = 2 TO IN
   W02(J) = (W0(J + 1) - 2 * W0(J) + W0(J - 1)) / DX2
 NEXT J
W02(IP) = 0

REM # DEFINE CONSTANTS
C1 = H * H / 12
C2 = E * H
C3 = V * H
C4 = D * H
C5 = H * H * H / 12
C6 = 1 / (4 * DX2)
C7 = DT2 / C4
C9 = C7 / DX2

REM ######## DEFINE MATRIX "A" FOR ROTARY INERTIA
FOR J = 2 TO IN
```

```
A(J, J) = 1 + (2 * C1 / DX2)
IF J < IN THEN A(J, J + 1) = -C1 / DX2
IF J > 2 THEN A(J, J - 1) = -C1 / DX2
NEXT J

REM ##########################################################
REM ##########################################################
FOR I100 = 1 TO I9

N0 = N9(I100)
WMAX1 = 0
XMAX1 = 0
KAMAX1 = 0
UMAX = 0

REM # INITIAL CONDITIONS

FOR J = 1 TO IP
W(J, 1) = W0(J)
W(J, 2) = W0(J)
U(J, 1) = 0
U(J, 2) = 0
EP(J, 1) = 0
KA(J, 1) = 0
EP(J, 2) = 0
KA(J, 2) = 0
EPD(J) = 0
KAD(J) = 0
NEXT J


2500 REM # SIMPLY SUPPORTED BOUNDARY CONDITIONS
U(IP, 1) = 0: U(IP, 2) = 0: U(IP, 3) = 0
W(1, 1) = 0: W(1, 2) = 0: W(1, 3) = 0
W(IP, 1) = 0: W(IP, 2) = 0: W(IP, 3) = 0
MX(1) = 0: MX(IP) = 0
KA(1, 1) = 0: KA(1, 2) = 0: KA(IP, 1) = 0: KA(IP, 2) = 0
KAD(1) = 0: KAD(IP) = 0
WXX(1, 1) = 0: WXX(1, 2) = 0: WXX(IP, 1) = 0: WXX(IP, 2) = 0

REM##########################################################
REM ##########################################################
```

```
REM ## DEFINE ARRAYS
REM ## UX IS FIRST DERIVATIVE OF U
REM ## WX IS FIRST DERIVATIVE OF W
REM ## WXX IS SECOND DERIVATIVE OF W
REM ## NXX IS FIRST DERIVATIVE OF NX
REM ## MXXX IS SECOND DERIVATIVE OF MX

NX(1) = -N0 * SIN(PI * DT / T)
EP(1, 2) = NX(1) / (C2 + (C3 / DT))
U(1, 2) = -EP(1, 2) * DX / I2

FOR J = 1 TO IP
  WX(J, 1) = W01(J)
NEXT J

FOR J = 1 TO IP
  WXX(J, 1) = W02(J)
NEXT J

4000 REM ###############main subroutine####################
4001 REM ######################################################

FOR Q& = 2 TO NT&
TIME = (Q& - 1) * DT


 UX(1) = (U(2, 2) - U(1, 2)) / DX
 WX(1, 2) = W(2, 2) / DX
 WXX(1, 2) = 0: REM # HINGED AT 1
FOR J = 2 TO IN
 UX(J) = (U(J + 1, 2) - U(J - 1, 2)) / (2 * DX)
 WX(J, 2) = (W(J + 1, 2) - W(J - 1, 2)) / (2 * DX)
 WXX(J, 2) = (W(J + 1, 2) - 2 * W(J, 2) + W(J - 1, 2)) / DX2
NEXT J
 UX(IP) = -U(IP - 1, 2) / DX
 WX(IP, 2) = -W(IN, 2) / DX
 WXX(IP, 2) = 0: REM # FOR HINGED AT IP


FOR L = 2 TO IN
 EP(L, 2) = UX(L) + .5 * (WX(L, 2) ^ 2 - W012(L))
 EPD(L) = (EP(L, 2) - EP(L, 1)) / DT
```

```
 KA(L, 2) = WXX(L, 2) - W02(L)
 KAD(L) = (KA(L, 2) - KA(L, 1)) / DT
 NX(L) = C2 * EP(L, 2) + C3 * EPD(L)
 MX(L) = C5 * (E * KA(L, 2) + V * KAD(L))
NEXT L


 EP(IP, 2) = UX(IP) + .5 * (WX(IP, 2) ^ 2 - W012(IP))
 EPD(IP) = (EP(IP, 2) - EP(IP, 1)) / DT
 KA(IP, 2) = 0
 KAD(IP) = 0
 NX(IP) = C2 * EP(IP, 2) + C3 * EPD(IP)

 NXX(1) = (NX(2) - NX(1)) / DX
 MXXX(1) = (MX(3) / 2 - MX(2)) / DX2
FOR J = 2 TO IN
 NXX(J) = (NX(J + 1) - NX(J - 1)) / (2 * DX)
 MXXX(J) = (MX(J + 1) - 2 * MX(J) + MX(J - 1)) / DX2
NEXT J
 NXX(IP) = (NX(IP) - NX(IN)) / DX
 MXXX(IP) = (-MX(IN) + MX(IP - 2) / 2) / DX2


FOR L = 2 TO IN
 U(L, 3) = 2 * U(L, 2) - U(L, 1) + C7 * NXX(L)
NEXT L
 U(IP, 3) = 0


FOR L = 2 TO IN
 RHS1(L) = 2 * W(L, 2) - W(L, 1)
 RHS2(L) = R% * (C1 * (WXX(L, 1) - 2 * WXX(L, 2)))
 RHS3(L) = C7 * (-MXXX(L) + NX(L) * WXX(L, 2) + NXX(L) * WX(L, 2))
 RHS(L) = RHS1(L) + RHS2(L) + RHS3(L)
NEXT L

IF R% = 0 THEN
 FOR J = 2 TO IN
  W(J, 3) = RHS(J)
 NEXT J
 GOTO 8000
END IF
```

```
REM # LOOP FOR GAUSSIAN ELIMINATION TO OBTAIN 'W'

P(2, 2) = 1
P(2, 3) = A(2, 3) / A(2, 2)
RH(2) = RHS(2) / A(2, 2)
FOR L = 3 TO IN
 FOR J = L TO IN
  DA(L, J) = A(L, J) - P(L - 1, J) * A(L, L - 1)
  P(L, J) = DA(L, J) / DA(L, L)
  RH(L) = (RHS(L) - A(L, L - 1) * RH(L - 1)) / DA(L, L)
 NEXT J
NEXT L

REM # BACK SUBSTITUTION

W(IP - 1, 3) = RH(IP - 1)
FOR J = IP - 2 TO 2 STEP -1
W(J, 3) = RH(J) - P(J, J + 1) * W(J + 1, 3)
NEXT J

8000


TIME1 = Q& * DT
NX(1) = -N0 * SIN(PI * TIME1 / T)
IF TIME1 >= T THEN NX(1) = 0
B1 = (U(2, 3) / DX) + .5 * ((W(2, 3) / DX) ^ 2 - W012(1))
U(1, 3) = (((C2 * B1) + (C3 / DT) * (B1 - EP(1, 2)) - NX(1)) / (C2 + (C3 / DT))) *
DX

REM ## TO FIND MAX DEFLECTION AND ITS LOCATION
REM ### IN THIS TIME STEP
XMAX = 0
WMAX = 0
FOR J = 1 TO IP
 IF ABS(W(J, 3)) > ABS(WMAX) THEN
 WMAX = W(J, 3)
 XMAX = (J - 1) * DX
 END IF
NEXT J

REM ## TO FIND MAXIMUM CURVATURE IN THIS TIME STEP
```

```
KAMAX = 0
FOR J = 1 TO IP
 IF ABS(KA(J, 2)) > ABS(KAMAX) THEN
 KAMAX = KA(J, 2)
 END IF
NEXT J

REM ## TO FIND MAXIMUM DISPLACEMENT

IF U(1, 3) > UMAX THEN UMAX = U(1, 3)

REM ## TO FIND OVERALL PEAK DEFLECTION

IF ABS(WMAX1) < ABS(WMAX) THEN
 WMAX1 = WMAX
 XMAX1 = XMAX
 TIMEMAX = TIME + DT
END IF

REM ## TO FIND OVERALL PEAK CURVATURE

IF ABS(KAMAX1) < ABS(KAMAX) THEN
 KAMAX1 = KAMAX
 TIKAMAX = TIME
END IF

REM # SHIFTING THE ARRAY IN TIME

FOR L = 1 TO IP
 U(L, 1) = U(L, 2)
 W(L, 1) = W(L, 2)
 W(L, 2) = W(L, 3)
 U(L, 2) = U(L, 3)
 EP(L, 1) = EP(L, 2)
 KA(L, 1) = KA(L, 2)
 WX(L, 1) = WX(L, 2)
 WXX(L, 1) = WXX(L, 2)
NEXT L

EP(1, 2) = (U(2, 2) - U(1, 2)) / DX + .5 * ((W(2, 2) / DX) ^ 2 - W012(1))
EPD(1) = (EP(1, 2) - EP(1, 1)) / DT
KA(1, 2) = (W(3, 2) - 2 * W(2, 2)) / DX2 - W02(1)
KAD(1) = (KA(1, 2) - KA(1, 1)) / DT
```

```
NEXT Q&

OPEN "C:\RESULT.DAT" FOR APPEND AS #1
PRINT #1, N0; ; WMAX1; ; XMAX1; ; TIMEMAX; ; KAMAX1; ; TIKAMAX; ;
UMAX
CLOSE #1


NEXT I100


STOP
```

Appendix B

Computer Program for Animation

```
REM #### B U C K L I N G  A N I M A T I O N  ###


REM ## DEFINE SCREEN COLOR, VARIABLE TYPE ETC.
SCREEN 12
COLOR 15
DEFDBL T
DEFINT I-J

PI = 4 * ATN(1)


REM ## PROGRAM INPUTS

REM ## FILES "A" AND "B" ARE .DAT FILES CONTAINING AN OUT PUT
REM ## FROM THE PROGRAM IN APPENDIX A. THE FILE CONTAINS
REM ## CERTAIN CONSTANT INPUTS IN THE FIRST LINE AND THE
REM ## NODAL DISPLACEMENT AND DEFLECTIONS

PRINT
INPUT "THE # OF SNAPSHOTS "; ISNAP
INPUT "HOW MANY LOAD CASES TO VIEW(1 or 2)="; IL
INPUT "NAME OF THE 1ST FILE?"; A$
IF IL = 2 THEN INPUT "NAME OF 2ND FILE ?"; B$
INPUT "INPUT TIME BETWEEN FRAMES "; TFRAME
PRINT A$

OPEN A$ FOR INPUT AS #1
INPUT #1, DT1, INTERVAL1, L, IN, W0, T, V1

IP = IN + 1

DIM X1(IP, ISNAP), Y1(IP, ISNAP), X2(IP, ISNAP), Y2(IP, ISNAP)

REM ### C A L C U L A T I O N ###

LSEG = (L / IN) * 400: REM *** VERTICAL SCALE IS 400PIXELS=1M
Y1(1, 1) = 20: REM ** TOP OF BEAM IS AT (100,20) ON SCREEN
X1(1, 1) = 100
FOR I = 2 TO IP
 Y1(I, 1) = (I - 1) * LSEG + 20
 X1(I, 1) = W0 * 1000 * SIN(PI * Y1(I, 1) / (100 * L)) + 100: REM (X SCALE 1
PIXEL = 1MM)
```

```
NEXT I

IF IL = 2 THEN
 FOR I = 1 TO IP
  X2(I, 1) = X1(I, 1) + 350: REM ** BEAM 2 IS 350 TO RIGHT OF BEAM1
  Y2(I, 1) = Y1(I, 1)
 NEXT I
END IF

CLS

FOR I = 2 TO ISNAP
 FOR J = 1 TO IP
 INPUT #1, X1(J, I), Y1(J, I)
 X1(J, I) = 1000 * X1(J, I) + 100: REM ** X Scale : 1 PIXEL = 1 MM
 Y1(J, I) = Y1(J, 1) + (400 * Y1(J, I))
 NEXT J
NEXT I

LSTEPS = T / DT1

IF IL = 2 THEN
OPEN B$ FOR INPUT AS #2
INPUT #2, DT2, INTERVAL2, L, IN, W0, T, V2
FOR I = 2 TO ISNAP
 FOR J = 1 TO IP
 INPUT #2, X2(J, I), Y2(J, I)
 X2(J, I) = 1000 * X2(J, I) + 450
 Y2(J, I) = Y2(J, 1) + (400 * Y2(J, I))
 NEXT J
NEXT I

END IF

LOCATE 1, 10: PRINT "V="; V1: LOCATE 1, 50: PRINT "V="; V2

VIEW (20, 20)-(620, 460), 8, 4
REM : NOW THE COORDINATES ARE WITH RESPECT TO (20,20)
FOR I = 1 TO ISNAP
 TIMEY = 460 - (50 * (INTERVAL1 * (I - 1) / LSTEPS))
 LINE (310, 410)-(330, 410), 4
 LINE (320, 460)-(320, TIMEY), 1
```

```
FOR J = 1 TO IN
 LINE (X1(J, I), Y1(J, I))-(X1(J + 1, I), Y1(J + 1, I))
 LINE (X2(J, I), Y2(J, 1))-(X2(J + 1, I), Y2(J + 1, I))
NEXT J

  NOW! = TIMER
  DO
  LOOP UNTIL TIMER > NOW! + TFRAME

  VIEW (20, 20)-(620, 460), 8, 4: REM refreshes the screen
NEXT I

STOP
```

BIBLIOGRAPHY

Ari-Gur, J., & Elishakoff, I. (1993). Dynamic Pulse Buckling of a Transversely Isotropic Column. Recent Advances in Structural Mechanics, ASME 1993, PVP-Vol. 269/ NE-Vol. 13, pp. 29-35.

Ari-Gur, J., Weller, T., & Singer, J. (1982). Experimental and Theoretical Studies of Columns under Axial Impact. Internal Journal of Solids Structures, Vol. 18, No. 7, pp. 619-641.

Budiansky, B., & Hutchinson, J.W. (1966). Dynamic Buckling of Imperfection Sensitive Structures. Proc. of the Eleventh International Congress of Applied Mechanics, Munich, Springer-Verlag, pp. 636-651.

Cederbaum, G., & Mond, M., (1992). Stability Properties of a Viscoelastic Column Under a Periodic Force. ASME Journal of Applied Mechanics, Vol. 59, pp.16-19.

Erickson, B., Nardo, S.V., Patel, S.A., & Hoff, N.J. (1956). An Experimental Investigation of the Maximum Loads Supported by Elastic Columns in Rapid Compression Tests. Proc. Society of Experimental Stress Analysis, Vol. 14, pp. 13-20.

Goldsmith, W. (1960). Impact. Edward Arnold.

Hayashi, T., & Sano, Y. (1972a). Dynamic Buckling of Elastic Bars, 1st Report, The Case of Low Velocity Impact. Bulletin JSME, Vol. 15, No. 88, pp. 1167-1175.

Hayashi, T., & Sano, Y. (1972b). Dynamic Buckling of Elastic Bars, 1st Report, The Case of High Velocity Impact. Bulletin JSME, Vol. 15, No. 88, pp. 1176-1184.

Hoff, N.J. (1953). The Dynamics of the Buckling of Elastic Columns. ASME Journal of Applied Mechanics, Vol. 17, No. 1, pp. 68-74

Koning, V.C., & Taub, J. (1933). Impact Buckling of Thin Bars in the Elastic Range Hinged at Both Ends. Luftfahrtforschung, Vol.10, No. 2.

Lindberg, H.E., & Florence, A.L. (1987). Dynamic Pulse Buckling (Ch. 2). Martinus Nijhoff Publ.

Meier, J.H. (1945). On Dynamics of Elastic Buckling. Journal of Aeronautical Science, Vol. 12, pp. 433-440.

Sevin, E. (1960). On the Elastic Bending of Columns due to Dynamic Axial Forces Including Effects of Axial Inertia. ASME Journal of Applied Mechanics, Vol. 27, No.1, pp. 125-131.

Smith, G.D. (1969). Numerical Solution of Partial Differential Equations. Oxford.

Thomson, W.T. (1988). Theory of Vibrations with Applications. Prentice Hall.

Vinogradov, A.M. (1987). Buckling of Viscoelastic Beam Columns. AIAA Journal, Vol. 25, No. 3, pp. 479-483.